Chapter 1

Introduction

1.1 Background

Because optical fibers offer much higher bandwidth than copper cables and are less susceptible to various kinds of electromagnetic interferences and other undesirable effects, optical networks are widely deployed today in all kinds of telecommunications. For past decades, fiber transmission technology has evolved to increase the transmission capacity. There are fundamentally two ways of increasing capacity on a fiber, as shown in Fig.1-1.

The first is to increase the bit rate. This requires higher-speed electronics. Many lower-speed data streams are multiplexed into a higher-speed stream at the transmission bit rate by means of electronics or optical *time division multiplexing* (TDM). An increase to 40 Gb/s is currently feasible, but this technology involves utilization of high-complexity components, with technological and physical impairments regarding group velocity and polarization mode dispersion in fiber, leading to limitation on the achievable transmission distance. [1]

Another way to increase the capacity is by a technique called *wavelength division multiplexing* (WDM). This optical technology couples many wavelengths in the same fiber, thus effectively increasing the aggregate bandwidth per fiber to the sum of the bit rates of each wavelength. For example, 40 wavelengths at 10Gb/s per wavelength in the same fiber raise the aggregate bandwidth to 400Gb/s. To date, an astonishing aggregate bandwidth at several Tb/s is also a reality.

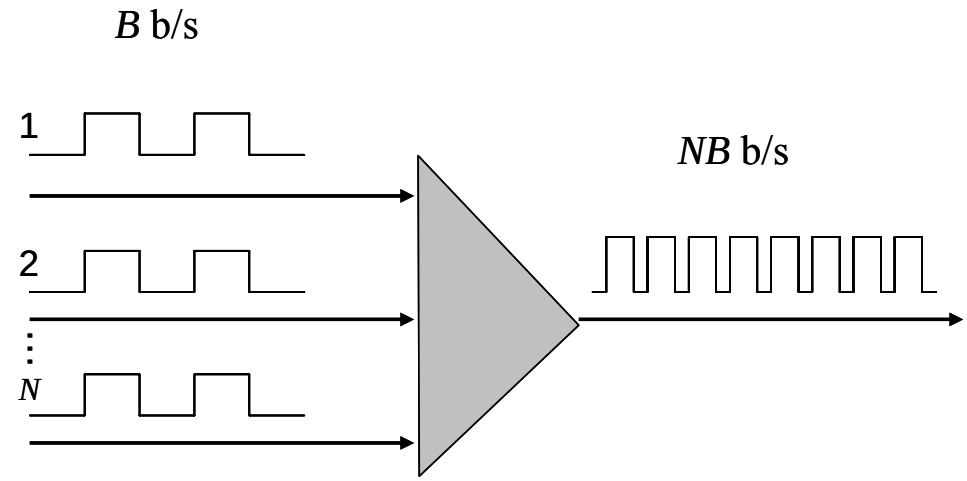

(a)

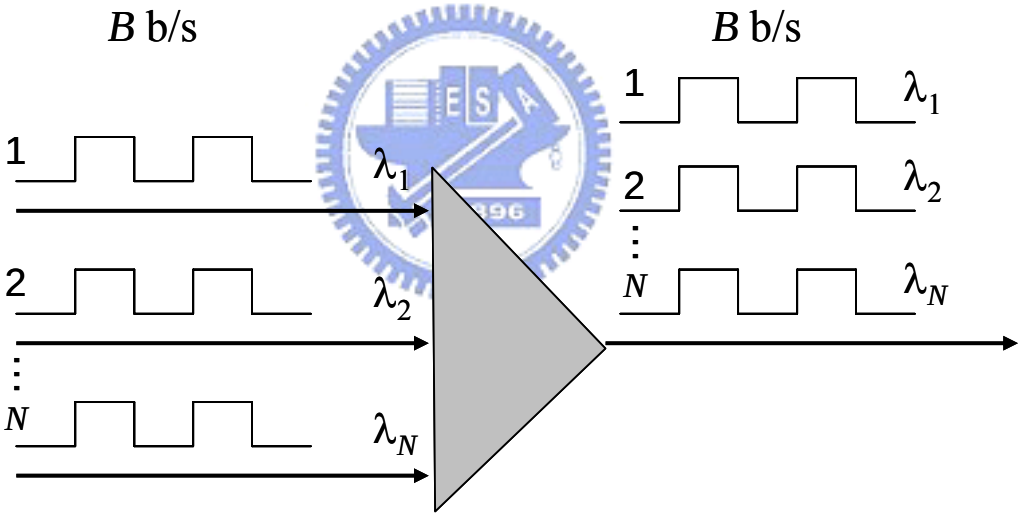

(b)

Fig. 1-1 Two different multiplexing techniques for increasing the transmission capacity on an fiber. (a) Electronic or optical time division multiplexing and (b) wavelength division multiplexing

Dense WDM (DWDM), with larger number of wavelength coupled into a fiber than WDM, is a successful system that allows the construction of long-haul transmission networks. This technology is largely due to the development of erbium-doped fiber amplifier (EDFA), an optical device that uses energy from a laser pump to amplify all signal wavelengths presented to its input.

DWDM systems take advantages of advanced optical technology (e.g., tunable lasers, narrow-band optical filters, ect.) to generate many wavelengths in the range around 1550nm. However, as the number of wavelengths increases, several issues need attention, such as channel spacing, bandwidth and channel shape, Insertion loss, crosstalk, and so on. We define these terms as follow: [2]

(1) Number of Channels

The number of non-overlapping channels is a straightforward parameter. How many channels can the unit separate in the spectrum depend on the channel center frequency and width.

(2) Channel spacing

The channel spacing, which is the minimum frequency separation between two adjacent channels, is required to guarantee minimum crosstalk effect. The International Telecommunications Union (ITU) has defined standard channel spacing of 200GHz and 100 GHz. Now channel spacing on a 50 GHz or 25 GHZ grid is being developed.

(3) Bandwidth and channel shape

The actual shape will determine the requirements on the laser stability. That is, the more pointed or rounded the shape the more variation in the laser wavelength will affect system performance. Typical laser requirements for 50 GHz systems are ±100

pm. The ideal shape is a flat top with very steep sides. The band shape can be characterized by a figure of merit defined as:

$$FOM = \frac{bandwidth\,@\,0.5dB}{bandwidth\,@\,25dB}$$

In the ideal case the FOM = 1, but in most practical cases the FOM < 0.5.

The net or clear channel bandwidth is then defined as:

Net bw = Measured bw- (ITU wavelength – Center wavelength) - Temperature drifts

(4) Insertion loss (IL)

The insertion loss should be specified with regard to the polarization state. This implies knowledge of the polarization properties of the source. An unpolarized source will give the average insertion loss, while a polarized source will provide an arbitrary value. A complete characterization of the insertion loss would include both the polarization and temperature dependence.

(5) Crosstalk

Almost every component in a WDM system introduces crosstalk of some form or another. The components include filters, wavelength multiplexers/demultiplexers, switches and semiconductor optical amplifiers. Two forms of crosstalk arise in WDM systems: interchannel crosstalk and intrachannel crosstalk. The first case is when the crosstalk signal is at a wavelength sufficiently different from the desired signal's wavelength that the difference is larger than the receiver's electrical bandwidth. This form of crosstalk is called interchannel crosstalk. The second case is when the crosstalk signal is at the same wavelength as that of desired signal or sufficiently close to it that the difference in wavelength is within the receiver's electrical bandwidth.

This form of crosstalk is called intrachannel crosstalk or sometimes, coherent crosstalk. Intrachannel crosstalk effects can be more severe than interchannel crosstalk, as we will see. In both cases, crosstalk results in a power penalty.

(6) Polarization Dependence

Many of the parameters such as bandwidth, center wavelength, and insertion loss are dependent on the state of polarization. As the polarization varies the shape of the demultiplexer function will change. It is important to map the changes in the spectrum for all the polarization states across the entire band. As the channel shape changes the center wavelength can shift and the insertion loss will vary. This can cause increased crosstalk or a reduction in the link margin.

(7) Wavelength stabilization

Among all kinds of laser sources in WDM, distribute-feedback (DFB) lasers are required in almost all high-speed transmission systems today due to its high power and narrow linewidth. The temperature sensitivity of a semiconductor DFB laser operating at the 1550nm wavelength region is about 0.1nm/ °C. The laser comes packaged with a thermistor and a thermoelectric (TE) cooler. The temperature can be sensed by monitoring the resistance of the thermistor and can be kept constant by adjusting the drive current of the TE cooler. However, the center wavelength of laser will change because of aging effects over a long period. Besides, ultra DWDM with channel spacing < 50GHz is the trend of future, so we must use some effective techniques to stabilize the frequency of DFB laser.

In the next section, we will list some previous methods for DFB laser diode frequency stabilization.

1.2 Previous methods

Various locking methods can achieve laser frequency stabilization. Four examples are as follows [3]:

1. Lock DFB laser to atomic transition lines.

Fig. 1-2 shows the basic concept of locking a DFB laser to an atomic transition, in this case using argon as the atom [4]. A small gas-filled lamp is used to generate the atomic line, and the laser can be rigidly locked to any desirable wavelength in relation to the atomic line. This method ensures that a signal channel will not drift.

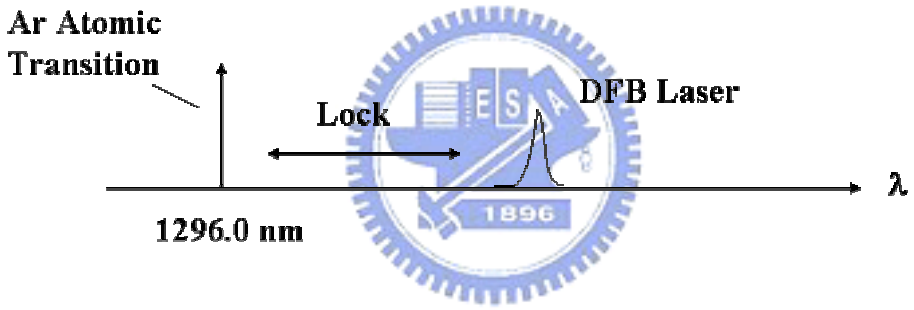

Fig. 1-2 Locking a DFB to a wavelength relative to atomic transition line

2. Lock DFB laser to molecular absorption lines

Besides locking to atomic transition, absolute frequency stability achieved by locking to molecular absorption line has been implemented. In the reference [5], it describes a frequency-stabilized DFB laser diode module by using a vibrational-rotational absorption of acetylene (C_2H_2) at the 1531.59 nm wavelength. Fig. 1-3 shows the transmission spectrum of $^{13}C_2H_2$ (10 cm optical path, 50 Torr pressure, and room temperature). Also, the frequency stabilization is carried out by direct modulation of the injection current applied to the DFB laser.

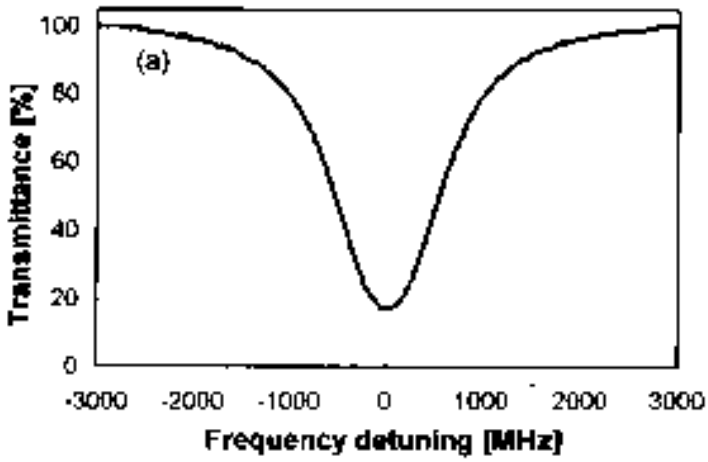

Fig. 1-3 Transmission spectrum of the vibrational-rotational line of $^{13}C_2H_2$

3. Use Fabry-Perot interferometers.

In this approach, the laser frequency is locked to the slope of the transmission or of the reflection peak of a Fabry-Perot interferometer (FPI) as frequency discriminator. Frequency variations in the laser can thus be converted to amplitude variations in the photocurrent. From a comparison of the photocurrent with a reference, a difference signal for the feedback loop is derived which is proportional to the instantaneous frequency deviation of the laser.

4. Use Fiber grating.

In the reference [6], a novel and effective way of frequency stabilization of DFB laser using a fiber grating is proposed. Their scheme is based on a level detection technique using the transmission and the reflection profiles of the fiber grating. The frequency stabilization is improved by two times compared with the DFB on unstable state. Besides, another frequency stabilization method using a fiber grating is described in reference [7]. They employ electronic feedback of the frequency error signal and utilize an in-fiber Bragg grating Fabry-Perot interferometer

as a frequency discriminator. The peak-to-peak drift of frequency is reduced to 60MHz for a period of 2.5hr.

1.3 Motivation and objectives

In order to increase transmission capacity, DWDM technology with channel spacing of 50GHz or less is now becoming the global trend in optical fiber communication. Because of tight channel spacing, laser sources with high wavelength stability are necessary. Several techniques we introduced in chapter 1.2 have been suggested to stabilize the DFB semiconductor laser. However, they still have some disadvantages. Locking to an atomic transition lines or molecular absorption lines prevent flexibility in the choice of operating wavelength. Optical feedback systems suffer some problems of instability [8].

Our scheme uses a fiber Bragg grating for DFB laser diode frequency stabilization. It is more suitable and effective way for DWDM network applications due to the fiber-based nature of architecture [6][7]. Moreover, it does not require complex electronics and dithering signals.

After frequency stabilization of DFB laser diode, we do the experiment of injection locking of an external-cavity laser (ECL) by the stabilized DFB and observe the output wavelengths variation of ECL. We expect that the frequency fluctuation of ECL output will be reduced. In addition, if the ECL has multiple output wavelengths, we try to lock one of the wavelengths by injecting locking technique, we expect the other wavelengths will be locked at the same time.

1.4 Organization of the thesis

In this thesis, we have developed a frequency-stabilized of DFB laser diode by using a fiber Bragg grating and injection locking of an external-cavity laser by the stabilized DFB laser. The outline of the thesis is as follows.

Chapter 1 begins with a basic review of WDM technology. Chapter 2 introduces the basic concept of fiber Bragg grating and basic theory of injection locking of semiconductor lasers. The circuit descriptions and experimental results of frequency stabilization of a DFB laser diode using a fiber Bragg grating are given in Chapter3. Chapter 4 describes the experimental setup and results of injection locking of an external-cavity semiconductor laser by the stabilized DFB laser. Finally, Chapter 5 gives the conclusions and future work.

Chapter 2

Basic Concept

In this chapter, we introduce the basic concepts of fiber Bragg grating and injection locked semiconductor laser. Sect. 2.1 gives the characteristics of fiber Bragg grating. Sect. 2.2 gives the basic theory of injection locking of semiconductor laser.

2.1 Fiber Bragg grating

2.1.1 Introduction

The fiber grating whose core refraction index varies along its length has developed into a critical component for many applications in fiber-optic communication and sensor systems [9]. Fiber grating can be broadly classified into two types: short-period grating (also called fiber Bragg grating or reflection grating) and long-period grating (also called transmission grating). Fig. 2-1 illustrates a short-period grating. The beam is reflected by a Bragg grating of a mode with a bounce angle θ_1 into the same mode traveling in the opposite direction with a bounce

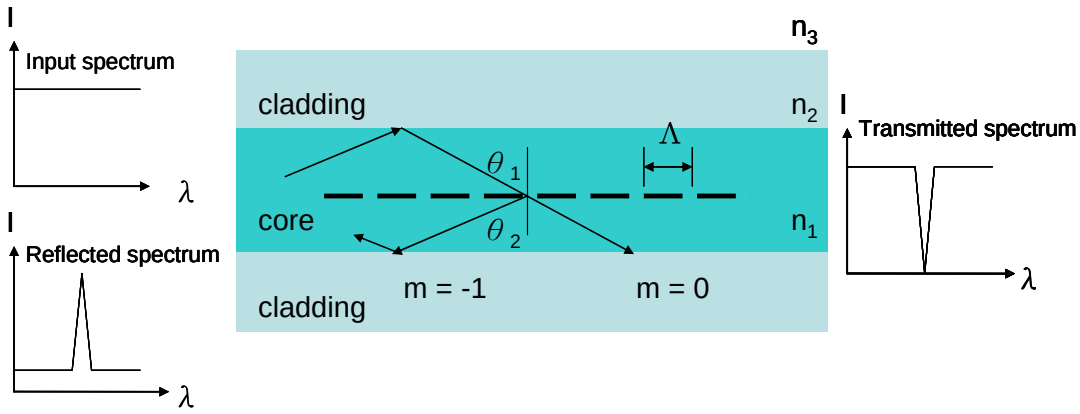

Fig. 2-1 Illustration of a fiber Bragg grating (reflection grating)

angle $\theta_2 = -\theta_1$. For reflected spectrum, we can find there is a λ, which satisfies the Bragg condition appearing a peak value, and at the same position of wavelength in transmission spectrum disappears.

Diffraction by a transmission grating of a mode with a bounce angle of θ_1 into a co-propagating mode with a bounce angle of θ_2 is illustrated in Fig. 2-2. We find that there is no reflection in the reflected spectrum.

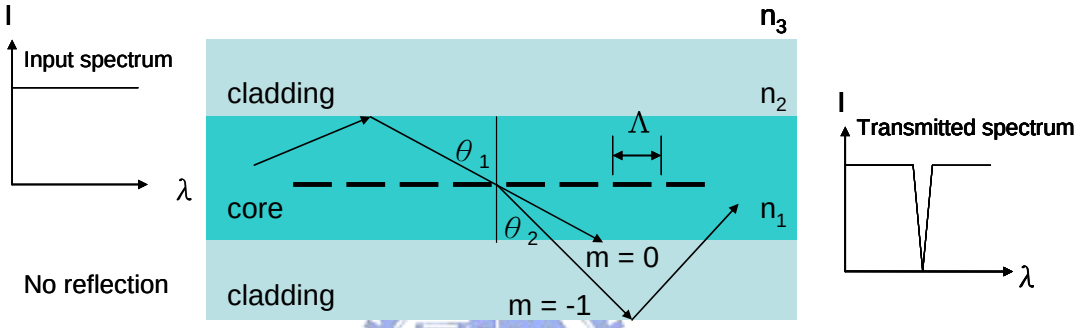

Fig. 2-2 Illustration of a fiber Bragg grating (transmission grating)

2.1.2 Fabrication of fiber Bragg grating

We focus on the fiber Bragg grating because we use it in our experiment. A fiber Bragg grating (FBG) consists of a fiber segment whose index of refraction varies periodically along its length. A periodic variation of the refractive index is formed by exposing the germano-silicate core of the fiber to an intense ultraviolet (UV) optical interference pattern that has a periodicity equal to the periodicity of the grating to be formed [5]. When the fiber is exposed to the intense UV pattern, structural defects are formed and thus a permanent variation of the refractive index having the same periodicity with the UV pattern. Fig. 2-3 illustrates an FBG using the UV method.

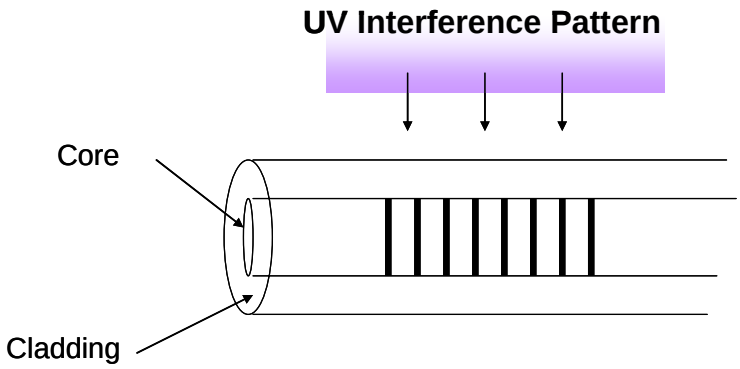

Fig. 2-3 A Bragg grating made by exposing a fiber with a UV pattern

The interference pattern has a periodicity that depends on the wavelength band the FBG is designed to operate in. For near–infrared wavelengths of about 1.55μm, the grating is made with a periodicity, d, of 1 to 10μm. The UV pattern is formed with one of several optical methods (diffraction or interferometry) that generate an interference pattern of alternating minima and maxima of light intensity. Regardless of the method used, the interference pattern must be of high quality with uniform periodicity, high contrast, and sharp edges.

The UV source is provided by an excimer laser that operates at a wavelength in the 157nm and 351nm range. The peak absorption is at 240nm and thus this wavelength is the most efficient. Escimer lasers may produce hundreds of milijoules in a 10-to-40nsec pulse, and can create the grating pattern in a fiber in a single high energy shot. Continuous wave (CW) laser sources at 1-watt output may also used.

2.1.3 Resonant wavelength for fiber Bragg grating

A fiber grating is simply an optical diffraction grating, and thus its effect upon a light wave incident on the grating at an angle θ_1 can be described by the familiar grating equation [9]

$$\boxed{n\sin\theta_2 = n\sin\theta_1 + m\frac{\lambda}{\Lambda}} \qquad (2.1)$$

Where θ_2 is the angle of the diffracted wave, n is the refractive index of medium, the integer m determines the diffraction order, and Λ is the period of the grating (see Fig. 2-4)

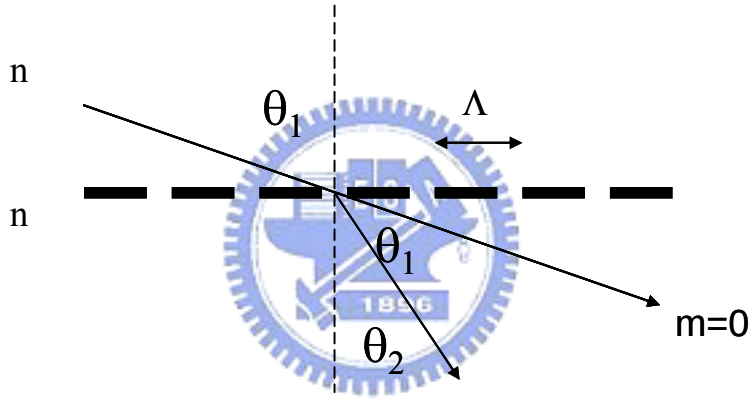

Fig. 2-4 The diffraction of a light wave by a grating

Consider a uniform fiber Bragg grating (see Fig. 2-1), the mode propagation constant β is simply $\beta = (2\pi/\lambda)\, n_{eff}$ where $n_{eff} = n_{co}\sin\theta$, we may rewrite equation (2.1) for guided modes as

$$\boxed{\beta_2 = \beta_1 + m\frac{2\pi}{\Lambda}} \qquad (2.2)$$

For first-order diffraction, which usually dominates in a fiber grating, m= -1. Recognizing $\beta_2<0$, we find that the resonant wavelength for reflection of a mode of index $n_{eff\,1}$ into a mode of index $n_{eff\,2}$ is

$$\boxed{\lambda = (n_{eff\,1} + n_{eff\,2})\Lambda} \tag{2.3}$$

If the two modes are identical, we get the familiar result for Bragg reflection:

$$\boxed{\lambda = 2n_{eff}\Lambda} \tag{2.4}$$

2.1.4 Coupled-mode theory

Coupled-mode theory is a very important tool for obtaining the reflection profile of fiber grating. In this thesis, we do not provide a derivation of this theory. We just list some useful formulas.

We assume the fiber Bragg grating is uniform along *z*. The index of refractive profile can be expressed as

$$\boxed{n(z) = n_0 + \Delta n \cos(\frac{2\pi z}{\Lambda})} \tag{2.5}$$

Where n_0 is average refractive index. Δn is the amplitude of the induced refractive index perturbation. By using coupled-mode theory of Lam and Garside in 1981 [10], that described the reflectivity of Bragg grating as

$$\boxed{R(l,\lambda) = \frac{\Omega^2 \sinh^2(sl)}{\Delta k^2 \sinh^2(sl) + s^2 \cosh^2(sl)}} \tag{2.6}$$

Where $R(l,\lambda)$ is the reflectivity that is function of the grating length l and wavelength λ. Ω is the coupling coefficient, $\Delta k = k - \pi / \lambda$ is the detuning wavevector, $k = 2\pi n_0 / \lambda$ is the propagation constant, $s^2 = \Omega^2 - \Delta k^2$. The coupling coefficient,Ω for sinusoidal variation of index perturbation along the fiber axis is given by

$$\boxed{\Omega \approx \frac{\pi \Delta n}{\lambda}(1 - \frac{\lambda}{2\pi a(n^2_{co} - n^2_{cl})})} \tag{2.7}$$

where a is the radius of core, n_{co} is the refractive index of core, n_{cl} is the refractive index of cladding, and Δn is the difference of n_{co} and $n_{cl.}$

At the central wavelength of fiber Bragg grating in reflection profile, there is no wavevector detuning, so $\Delta k=0$, the expression for the reflectivity becomes

$$\boxed{R(l,\lambda) = \tanh^2(\Omega l)} \tag{2.8}$$

The reflectivity increases as the induced index of refraction change increases. Similarly, as the length of the grating increases so does the resultant reflectivity. A calculated reflection spectrum as a function of the wavelength is shown is Fig. 2-5. [11] The side lobes of the resonance are due to multiple reflections to and from opposite ends of the grating region. The sine spectrum arises mathematically through the Fourier transform of a harmonic signal having finite extent; an infinitely long grating would transform to an ideal delta function response in the wavelength domain. A general expression for the approximate full-width-half-maximum bandwidth of a grating is given by

$$\boxed{\Delta\lambda = \lambda_B s\sqrt{(\frac{\Delta n}{2n_0})^2 + (\frac{1}{N})^2}} \tag{2.9}$$

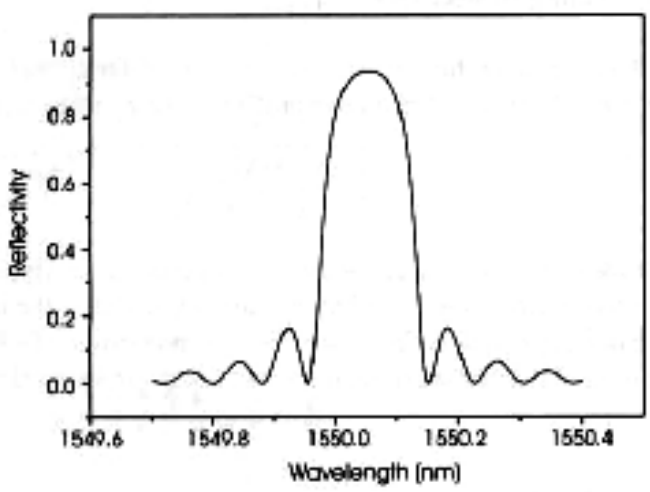

Fig. 2-5 Reflection spectrum of fiber Bragg grating

2.1.5 Strain and temperature sensitivity of fiber Bragg grating

The effective index of refraction of the core and periodicity of the grating will be affected by strain and temperature that will cause the shift of the Bragg grating center wavelength. Using equation (2.4) the shift in the Bragg grating center wavelength due to strain and temperature changes is given by

$$\boxed{\Delta\lambda_B = 2\left(\frac{\partial n_{eff}}{\partial l} + n_{eff}\frac{\partial \Lambda}{\partial l}\right)\Delta l + \left(\Lambda\frac{\partial n_{eff}}{\partial T} + n_{eff}\frac{\partial \Lambda}{\partial T}\right)\Delta T} \qquad (2.10)$$

We focus on the temperature effect. The fractional wavelength shift for a ΔT may be written as

$$\boxed{\Delta\lambda_B = \lambda_B(\alpha_\Lambda + \alpha_n)\Delta T} \qquad (2.11)$$

where $\alpha_\Lambda = (1/\Lambda)(\partial\Lambda/\partial T)$ is the thermal expansion coefficient for the fiber (approximately 0.55×10^{-6} for the silica), and $\alpha_n = (1/n_{eff})(\partial\, n_{eff}/\partial T)$ represents the thermo-optic coefficient, which is approximately equal to 8.6×10^{-6} for the germania-doped, silica-core fiber. From (2.11) the expected sensitivity for a 1550nm fiber Bragg grating is approximately 13.7pm/°C.

2.2 Injection locked semiconductor laser

2.2.1 Introduction

The observation of injection locking of oscillators can be traces back to 1665 when Huygens observed his wall two clocks for several days. He found when the two clocks were placed very close, the phenomenon of synchronism appeared [12][13]. The original analysis of injection locking was certain not done by Huygens since Newton's *Principia Mathmatica* was not published until 1687. Probably the earliest theoretical development of locking was present by Van der Pol in 1927 [14]. Nearly two decades later, Adler published a paper which provided a clear understanding of frequency locking phenomena [15]. The paper presented a nonlinear differential equation for the phase of an electrical oscillator relative to an injected signal. Adler showed that locking bandwidth was inversely proportional to the square root of the injected power.

It was not until 1966 that laser injection locking was demonstrated by Stover and Steiner [16].In 1973, Buczek provided a review of the theory and applications of laser injection locking [17]. In the late 1970's improvements in semiconductor laser characteristic such as improved spectral purity and mode stability provided motivation for injection locking these lasers. The first demonstration of semiconductor laser injection locking was presented in a paper by Kobayashi and Kimura in 1980 [18][19].

The theoretical developments for injection locking of semiconductor laser began in the early 1980's. Some researchers like Otsuka, Lang [20][21] discussed the linewidth and stability of an injection locked semiconductor laser. Then some applications of injection locking of semiconductor laser have been worked out on

optical communication [22]. It improved the dynamics of semiconductor lasers [21,23-26]. Recently, several research groups have shown theoretically that the injection locking technique can also increase the modulation bandwidth of semiconductor lasers, and hence improve the system performance at high frequencies [27]–[30].

2.2.2 Basic theory

Consider two semiconductor lasers illustrated in Fig 2-6, both emitting in a single longitudinal mode and with a very small difference in wavelength (or frequency). Light is injected from one laser, the master laser (ML), into the other laser, referred to as the slave laser (SL).

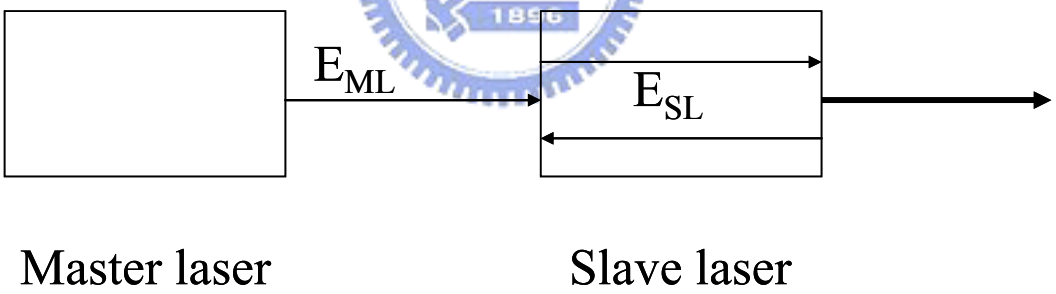

Fig. 2-6 Injection locking of semiconductor laser

We definite the emitted light of master laser is E_{ML} and emitted light of slave laser is $E_{SL.}$ We also assume the output of slave laser cannot be feedback to master laser. The theoretical analysis is based on the following equation for the complex electric field of the slave laser [21] [31]:

$$\Delta\widetilde{E}_{SL}(t) = j\varpi_{SL}(n)\widetilde{E}_{SL}(t)\tau_{RT} + \frac{1}{2}[G(n) - \frac{1}{\tau_p}]\widetilde{E}_{SL}(t)\tau_{RT} + \eta\widetilde{E}_{ML}(t) \quad (2\text{-}12)$$

$\Delta\widetilde{E}_{SL}(t)$ is the change of electric field of SL (slaver laser) for a round trip

w (n) and G(n) are the angular optical frequency and the modal gain per second of the SL, both depending an the carrier density *n*

$\varpi_{SL}(n) = \varpi_{SL0} + \frac{1}{2}\beta[G(n) - \frac{1}{\tau_p}]$ and $\varpi_{SL0} = \varpi(n_{th})$, n_{th} is the threshold carrier density, β is linewidth enhancement factor

τ_{RT} is the time for light of SL running for a round trip

$G(n) = G_N(n\text{-}n_0)$ is the gain of SL

τ_p is the phone lifetime

η is the coupling efficiency for ML inject to SL

We divide the equation (2-12) both side by τ_{RT} and assume $\Delta\widetilde{E}_{SL}(t)$ and τ_{RT} is small enough that can be neglected. A differential equation can be expressed as:

$$\frac{d}{dt}\widetilde{E}_{SL}(t) = j\varpi_{SL}(n)\widetilde{E}_{SL}(t) + \frac{1}{2}[G(n) - \frac{1}{\tau_p}]\widetilde{E}_{SL}(t) + \eta f_d\widetilde{E}_{ML}(t) \quad (2\text{-}13)$$

and $f_d = \frac{1}{\tau_{RT}}$ is the longitudinal mode spacing

The complex fields are represented by

$$\widetilde{E}_{SL}(t) = E_{SL}(t)e^{j[w_{SL}t + \phi_{SL}(t)]} \quad (2\text{-}14)$$

$$\eta\tilde{E}_{ML}(t) = E_{ML}(t)e^{j[w_{ML}t+\phi_{ML}(t)]} \tag{2-15}$$

By means of (2-14) and (2-15), (2-13) can be converted to the amplitude-phase representation

$$\frac{d}{dt}E_{SL}(t) = \frac{1}{2}[G(n) - \frac{1}{\tau_p}]E_{SL}(t) + f_d\sqrt{E_{ML}}\cos[\Delta(t)] \tag{2-16}$$

$$\frac{d}{dt}\phi_{SL}(t) = \frac{1}{2}\beta[G(n) - \frac{1}{\tau_p}] + f_d\frac{E_{ML}}{E_{SL}(t)}\sin[\Delta(t)] \tag{2-17}$$

and $$\Delta(t) = (\varpi_{ML} - \varpi_{SL})t - \phi_{SL}(t) \tag{2-18}$$

The carrier density must obey the usual rate equation

$$\frac{d}{dt}n(t) = J_e - \frac{n(t)}{\tau_{sp}} - G(n)E^2{}_{SL}(t) \tag{2-19}$$

J_e is the pumping term, and τ_{sp} is the spontaneous emission lifetime

Equations (2-16), (2-17), and (2-19) form the basic theoretical model for injection locking of semiconductor laser.

In the injection locked steady state, the two lasers must oscillate at the same frequency, and we can determine the locked phase ϕ_L of the slave laser relative to that of the master laser. This means that

$$\widetilde{E}_{SL}(t) = E_{SL}(t)e^{j[w_{ML}t+\phi_L]} \tag{2-20}$$

$$\phi_{SL}(t) = (\varpi_{ML} - \varpi_{SL})t + \phi_L \tag{2-21}$$

and from (2-18), we can obtain

$$\Delta(t) = -\phi_L \tag{2-22}$$

The stationary solutions to (2-16), (2-17), and (2-19) are found by further setting $E_{SL}(t)= E_{SL}$, then we obtain

$$\Delta\omega = -f_d \frac{E_{ML}}{E_{SL}}[\sin\phi_L + \beta\cos\phi_L] \tag{2-23}$$

By introducing

$$\Psi = \tan^{-1}\beta \tag{2-24}$$

(2-23) can be written as

$$\sin(\phi_L + \psi) = \frac{-\Delta\omega}{f_d \frac{E_{ML}}{E_{SL}}\sqrt{1+\beta^2}} \tag{2-25}$$

As can be seen, (2-25) can only be fulfilled if

$$|\Delta\omega| \le f_d \frac{E_{ML}}{E_{SL}}\sqrt{1+\beta^2} \tag{2-26}$$

where the locking half width is given by

$$\Delta\omega_L = f_d \frac{E_{ML}}{E_{SL}} \sqrt{1+\beta^2} \tag{2-27}$$

The linewidth enhancement factor β gives rise to an increase of the locking bandwidth with a factor of $\sqrt{1+\beta^2}$. However, part of this range may be dynamically unstable. In this thesis, we won't discuss this.

From (2-25) the locked phase can be determined as a function of the frequency detuning Δω

$$\phi_L = \left\{ \begin{array}{l} -\sin^{-1}\left(\frac{\Delta\omega}{\Delta\omega_L}\right) \\ \pi + \sin^{-1}\left(\frac{\Delta\omega}{\Delta\omega_L}\right) \end{array} \right\} - \psi + p \cdot 2\pi \tag{2-28}$$

where p is an integer. It can be shown that only the first solution with $d\phi_L / d(\Delta\omega)$ negative corresponds to an unconditionally stable steady state.

Confining ϕ_L to the interval [-π; π], the phase characteristic becomes

$$\phi_L = -\sin^{-1}\left(\frac{\Delta\omega}{\Delta\omega_L}\right) - \tan^{-1}\beta \tag{2-29}$$

The real locking range should include dynamically unstable [31]. We can use perturbation method and control theory to obtain dynamically stable locking range. However, it is complicated and some parameter of semiconductor is unknown. We will not discuss this in the thesis.

Chapter 3

Circuit description and experimental results of frequency stabilization for a DFB laser diode

In this chapter, we describe our method in frequency stabilization of a DFB laser diode using a fiber Bragg grating. Sect. 3.1 gives the experimental setup; Sect. 3.2 gives the experimental principle; Sect. 3.3 gives the results and discussions.

3.1 Experimental setup

The experimental setup is shown in Fig. 3-1. The DFB laser diode (Thorlabs. Inc ML925B11F) is drove by the current source (Newport, Model 505) and the temperature controller (Newport, Model 325) also works. The emitting laser is collimated by a collimated lens and then passes through an optical isolator to prevent feedback. We use two beam splitters to separate the laser beam into three ways. The first one is 50% intensity of DFB laser power as a laser output. The other two beams will do the level detection. One is directly incident on a photodetector (PD1) (Thorlabs, PDA400) and the variable attenuator controls the intensity of laser power. The other is incident on a fiber Bragg grating (made by opto-electronics & system laboratories of Industrial Technology Research Institute) then is detected with the other photodetector (PD2). (Thorlabs, PDA400) Error signal as a comparator output is fed back into DFB driving current after PI control. Because the FBG is easily affected by tension and temperature, we use type to bond FBG on Styrofoam, and cover it by another piece of Styrofoam.

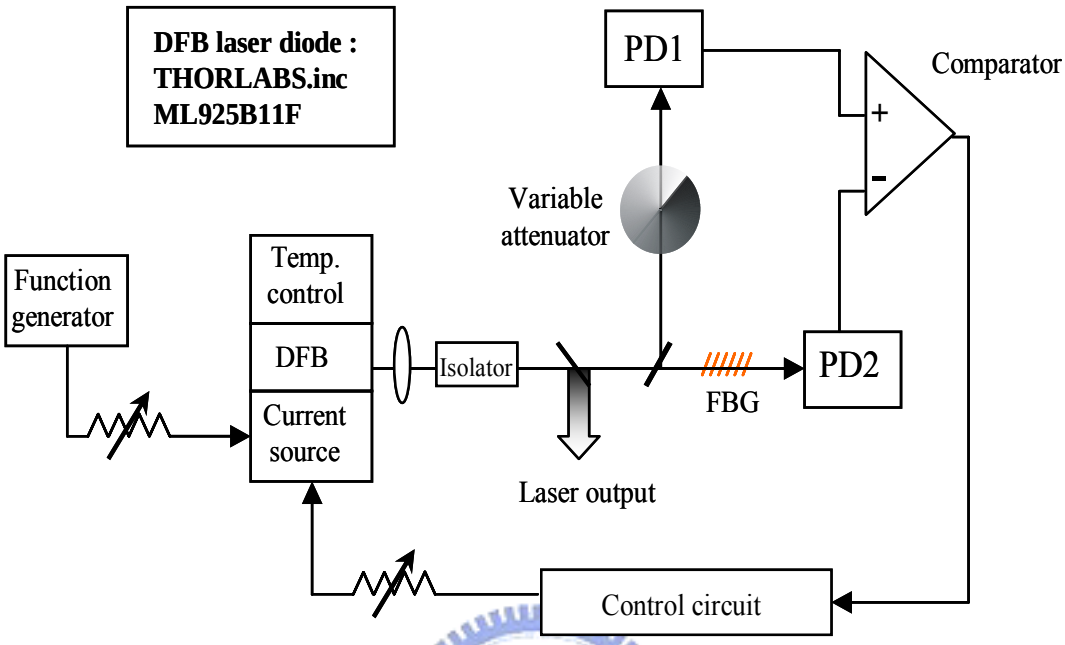

Fig. 3-1 The experimental setup of frequency stabilization of a DFB laser diode using a fiber Bragg grating

3.2 Operation principle

The transmission profile at room temperature 20° C of FBG with central wavelength 1547.71nm, FWHM = 0.16nm is shown in Fig.3-2.

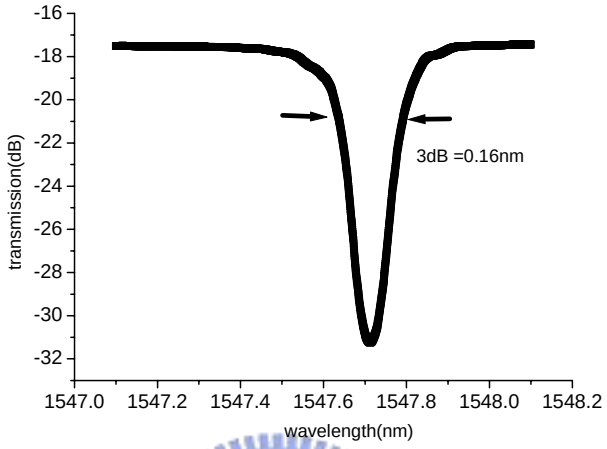

Fig. 3-2 The transmission profile of fiber Bragg grating

Fig. 3-3 shows the L-I curve of DFB laser diode at T =13°C. The threshold current is 7mA. Fig. 3-4 shows the spectrum of DFB laser with very narrow linewidth operating at I =20mA, T =20°C.

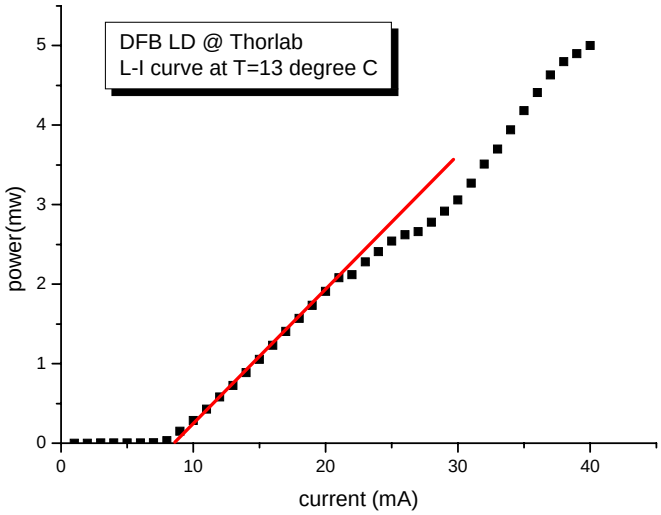

Fig. 3-3 The L – I curve of DFB laser diode

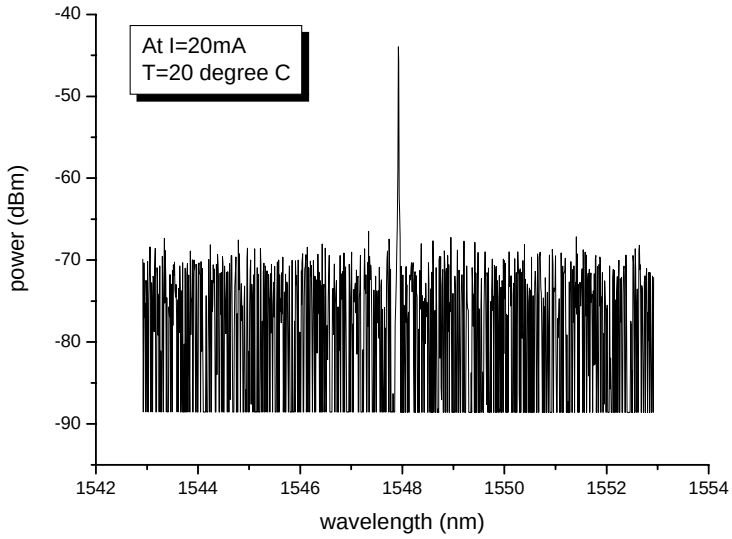

Fig. 3-4 The spectrum of DFB laser diode

We know that driving current and temperature controller varies the DFB wavelength, so we measure the wavelength tuning efficiency by current and temperature respectively. In Fig. 3-5 (a), at T = 20° C, wavelength shift linearly 0.019nm/ mA and in Fig. 3-5(b), at I =20mA, wavelength shift linearly 0.046nm/ °C.

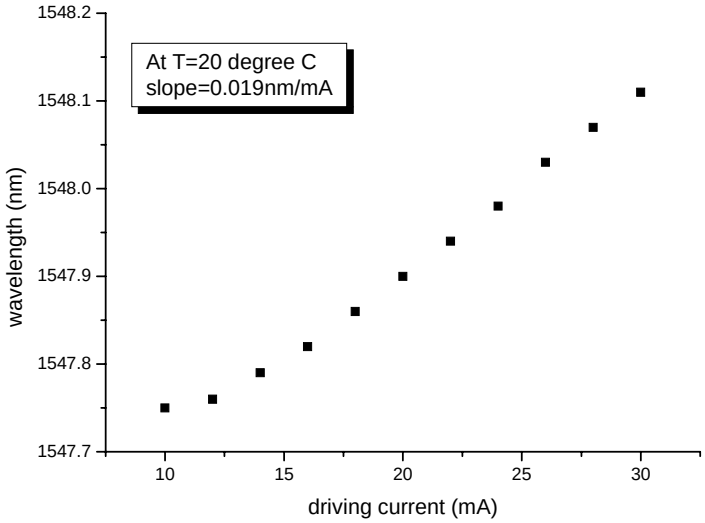

Fig. 3-5 (a) DFB wavelength tuning efficiency by driving current

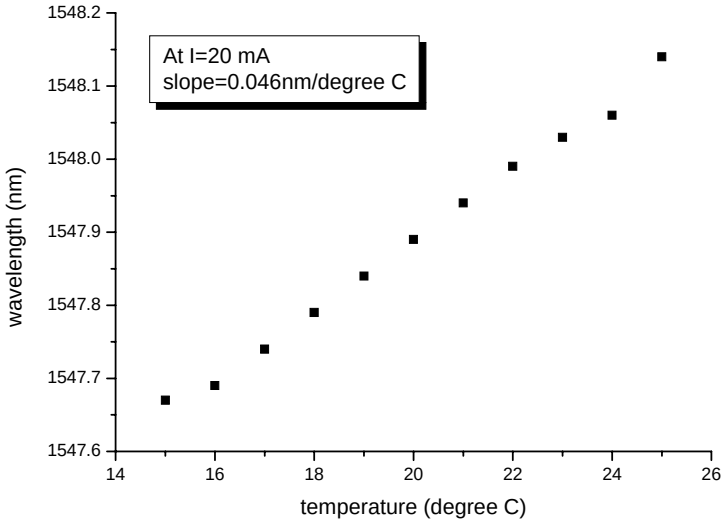

Fig. 3-5 (b) DFB wavelength tuning efficiency by temperature controller

In the beginning of our experiment, we would like to modulate the DFB temperature just like the reference [6]. After careful considering, we find that modulate the diving current is much easier and more effective than modulate the temperature controller. At T =13° C of DFB laser diode, we can find the range of wavelength drift changed by driving current can cover the FBG transmission spectrum. At T=13° C, wavelength tuning efficiency is 0.0209nm/mA is shown in Fig. 3-6.

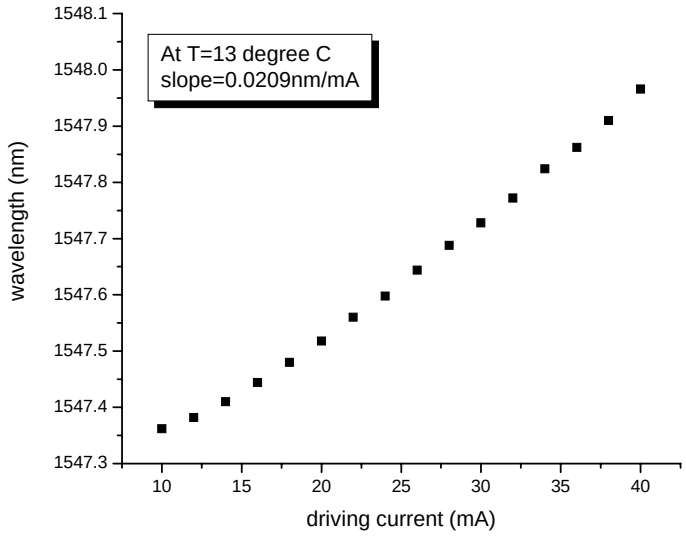

Fig. 3-6 DFB wavelength tuning efficiency by driving current

We use photo detector to recheck our modulation range. The emitted light of DFB goes though the FBG then measured by photodetector. By varying the drive current, the power variation of DFB output going through FBG will behave like a "filter" shown in Fig. 3-7.

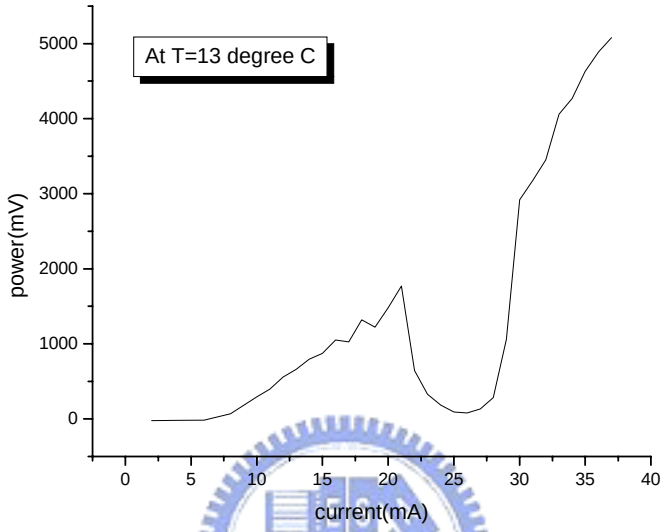

Fig. 3-7 Power variation of DFB going though FBG by tuning DFB driving current

Based on Fig.3-2, Fig.3-6, and Fig.3-7, the operation principle is illustrated in Fig 3-8. At the left side of Fig. 3-8, the dash line is non-transmission profile and solid line is transmission profile. The two signals are detected by two photo detectors (PD1 and PD2) and the comparator is used to compare them. We set λ_0 as the reference point. When the DFB drifts to longer wavelength ($\lambda > \lambda_0$), the control circuit will feedback negative current to the DFB to let wavelength drop back to λ_0. On the contrary, If DFB drifts to shorter wavelength ($\lambda < \lambda_0$), the control circuit will feedback positive current to the DFB to let wavelength pull back to λ_0

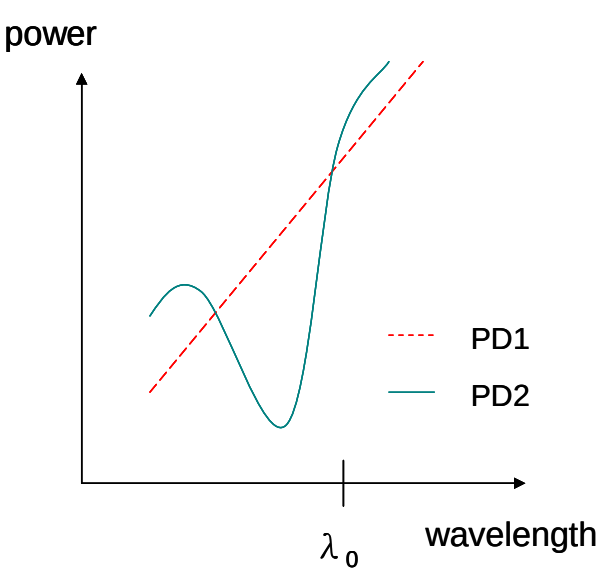

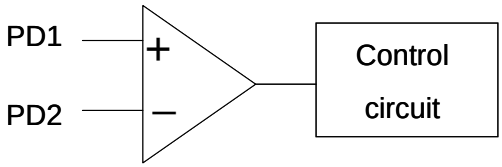

Comp	condition	action
0	OK	none
-	$\lambda > \lambda_0$	I ↓
+	$\lambda < \lambda_0$	I ↑

Fig. 3-8 Principle of experimental scheme

In order to find the proper reference point, a function generator and a variable attenuator are used. Our current source can be modulated 20mA by 1V input signal variation, so we set the function generator at ± 500mV, 1 KHz to change DFB current ± 10mA. In our experiment, DFB is set at I = 28±10mA and T =13°C to match the transmission profile of FBG. Fig. 3-9 shows power variation observed by oscillator. The dash line is measured by PD1 (see Fig.3-1), and the solid line is measured by PD2. The difference of PD1 and PD2 is shown in Fig. 3-10. Reference level we chose is at the zero point in Fig. 3-10. In other words, the point PD1=PD2 is our reference point. We can use variable attenuator to vary the power detected by PD1 to choose the reference point we like.

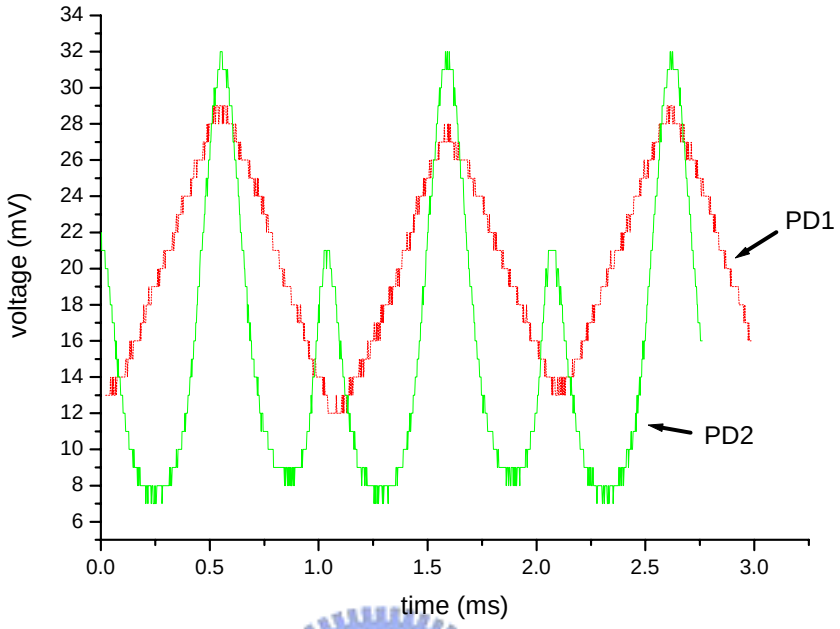

Fig. 3-9 The power variation using function generator

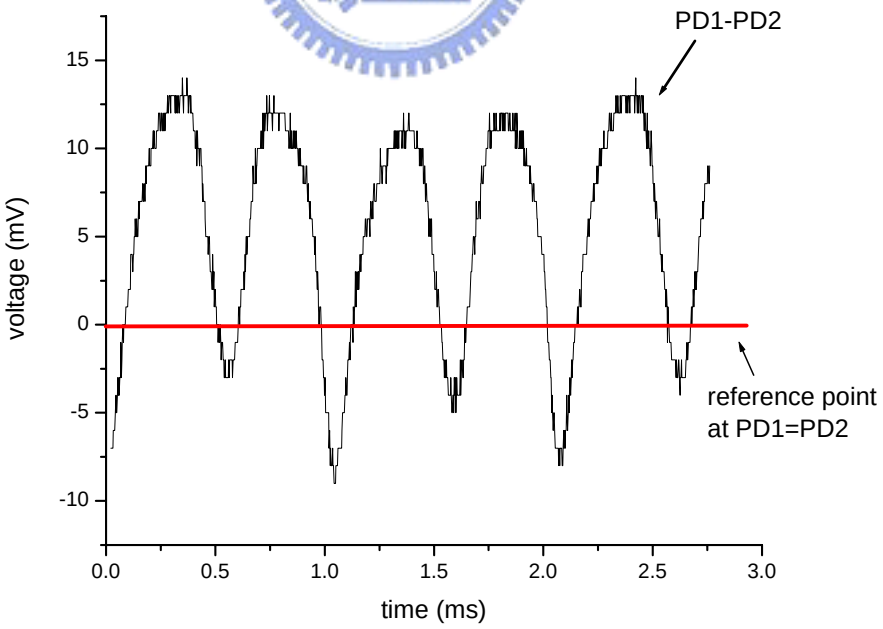

Fig. 3-10 The difference of PD1 and PD2 illustrated in Fig. 3-9

3.3 Experimental results

3.3.1 Short-term measurement

Error signal (PD1-PD2) is a simple index to observe whether the frequency is locked or not. We use oscilloscope that is adjusted to 1.25 sampling per second to observe the voltages of error signal on unstable state and on stable state. Fig. 3-11 illustrates the results. It's very easy to figure out that the frequency fluctuation of DFB is reduced after feedback circuit works.

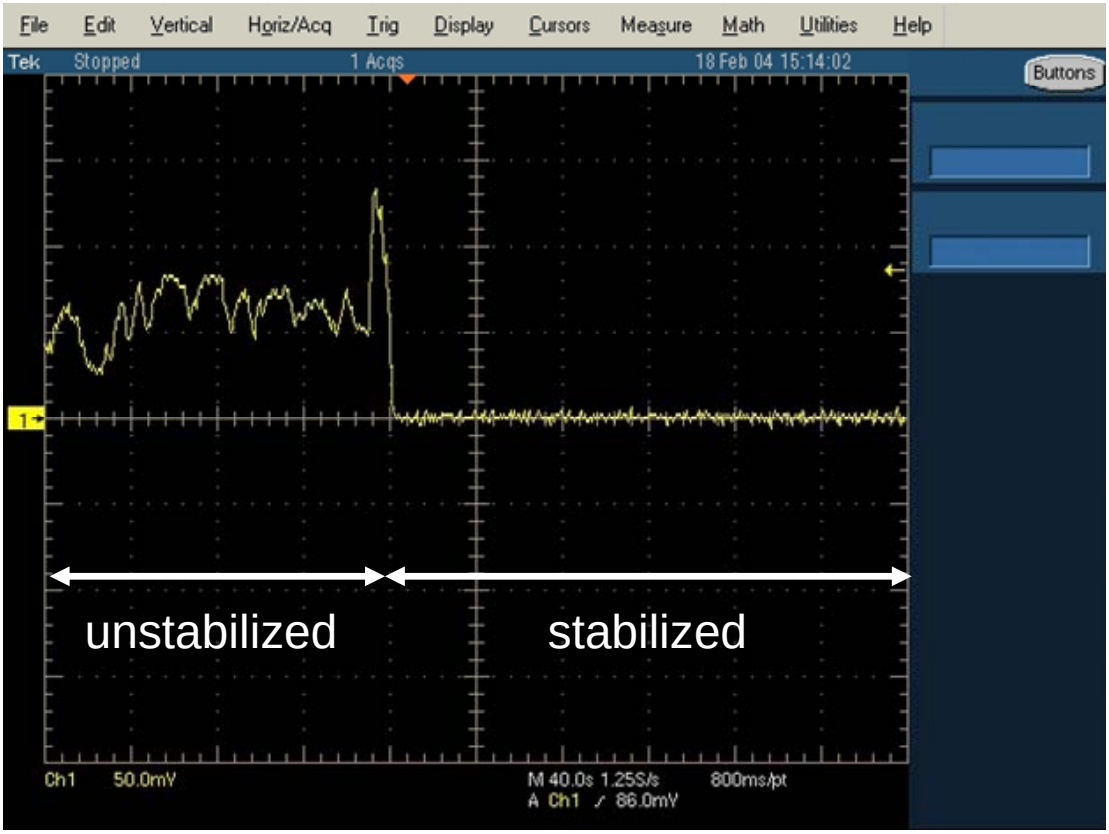

Fig. 3-11 Error signal on unstable state and on stable state

In order to calculate the frequency stability, while measuring the error signal on unstable state, we also measure the wavelength drift of DFB by wavemeter at the same time. We find in the unstable period over 2 minutes, the wavelength drift of DFB is 0.0007nm, shown in Fig. 3-12 and the error signal changes 60mV

(peak-to-peak). On stable state, the voltage changes 15mV that is four times lower than the voltages on unstable state, so we can infer that wavelength variation leads to 1.75×10^{-4}nm. By the formula calculation, the frequency fluctuation of the DFB is 22 MHz after stabilization for a short period of 4 minutes. The time constant of our integration controller is 0.01ms

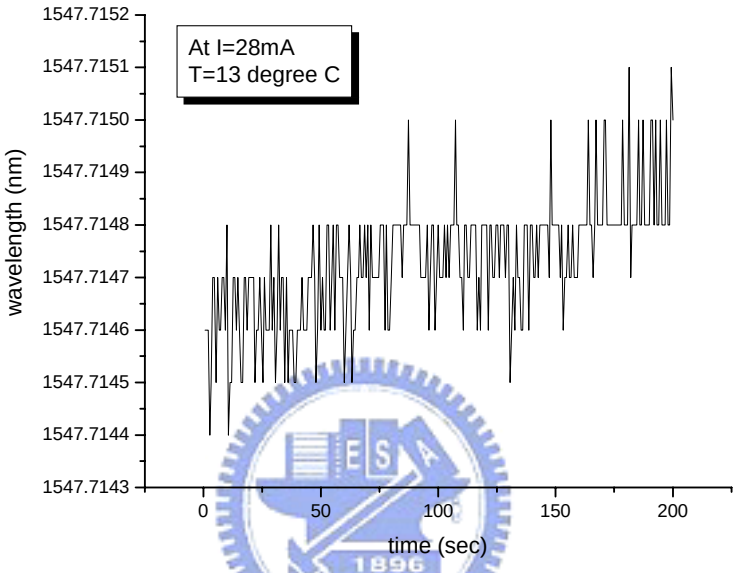

Fig. 3-12 Wavelength variation of DFB on free running state

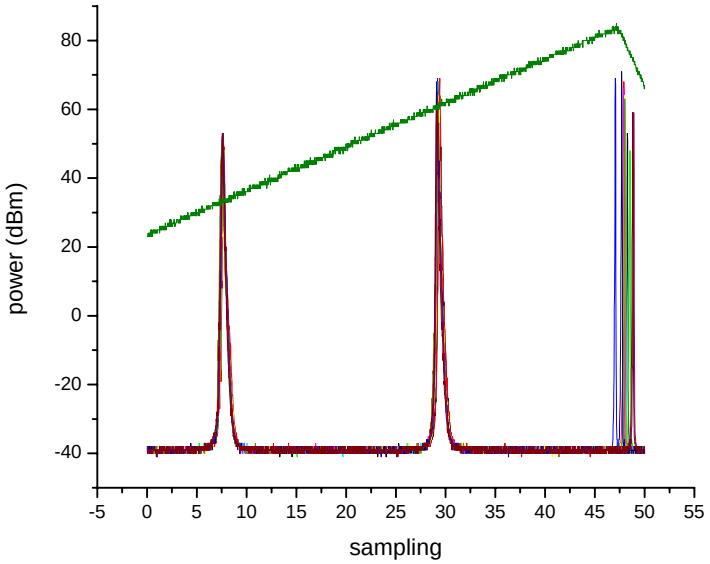

Fig. 3-13 Frequency stability measured by scanning Fabry-Perot interferometer

The scanning Fabry-Perot interferometer is also a meter for measuring short-term stability. The Fabry-Perot we use, FSR = 2GHz. We can find that the frequency stability shown in Fig. 3-13 is 36MHz for a period of 30 seconds.

3.3.2 Long-term measurement

For long-term measurement, we use multimeter to acquire the feedback voltages. Fig. 3-14 shows the results. Feedback voltage varies 0.57mV in the period of 2.5 hours. For our driving current machine, 1V input voltage can change 20mA and according to Fig. 3-6, the DFB wavelength tuning efficiency is 0.0209nm/mA. We can calculate the total wavelength shift is 2.38×10^{-4} nm. By formula calculation, the fluctuation of frequency is 29MHz.

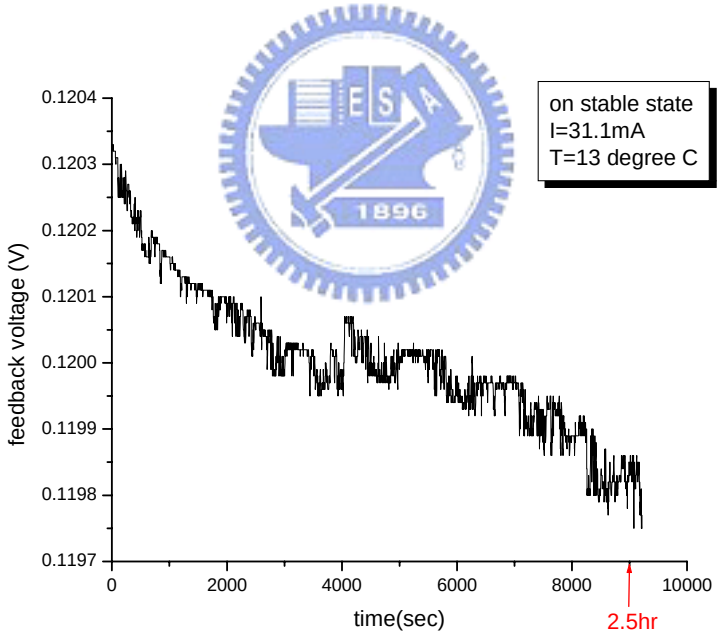

Fig. 3-14 Feedback voltage acquired by multimeter for a period of 2.5 hour

The feedback voltage can be affected by ambient temperature. Fig. 3-15 shows room temperature and the temperature surrounding FBG, respectively. As we know, one degree C variation in temperature will lead to 13.7 pm central wavelength shift of FBG.

Although, we package the FBG with Styrofoam, the temperature surrounding FBG goes gentler than room temperature; it still affects the FBG.

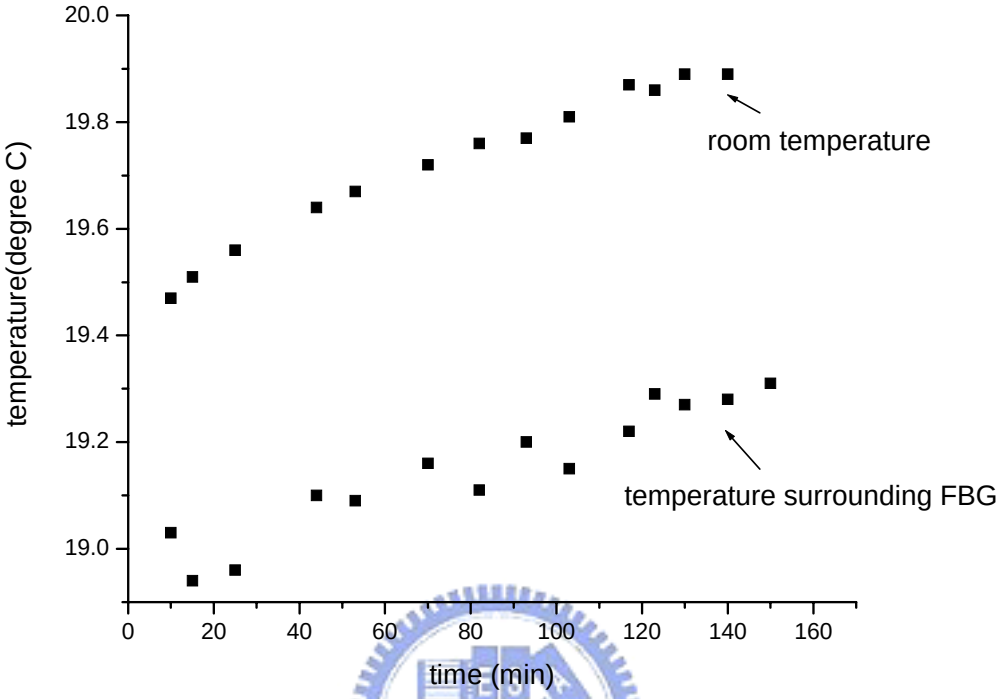

Fig. 3-15 temperature variation for over two hours

We can also use multimeter to acquire the voltage of error signal for a long time measurement. Just like we have mentioned before, we measure wavelength shift on unstable state while acquiring error signal. We compare the peak-to-peak voltage on stable state with the one on unstable state, and then wavelength shift on stable state can be calculated by using proportion. Fig. 3-16 shows the error signal for free running over 10 mins and Fig. 3-17 shows the DFB wavelength shift at the same time of measurement. We find that error signal changes 0.0165V while wavelength drifts 0.0024nm. Then we switch to the stable state. The error signal varies 0.00241V for a period of 17 hours shown in Fig.3-18. By calculation, the fluctuation of wavelength is 3.5×10^{-4}nm i.e. fluctuation of frequency is about 50MHz over 17hr.

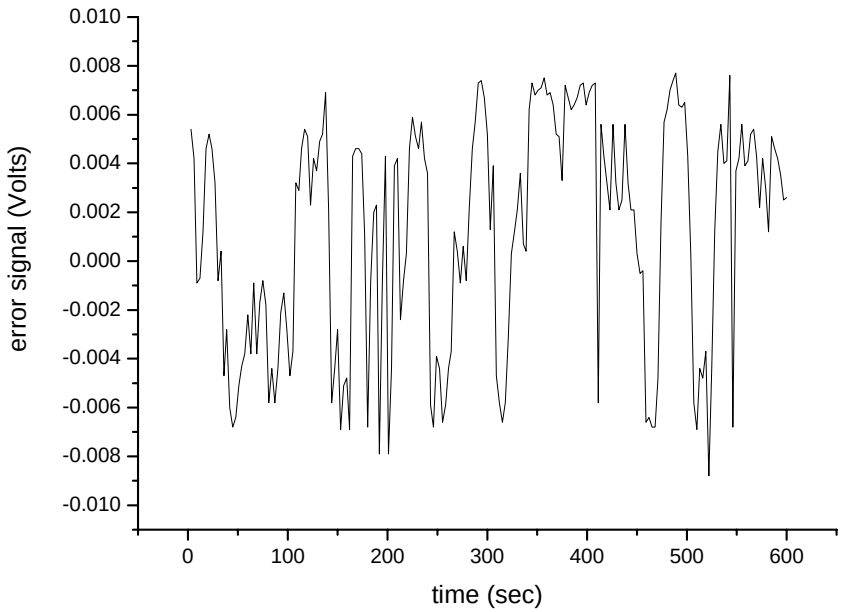

Fig. 3-16 Error signal without stabilization over 10 mins

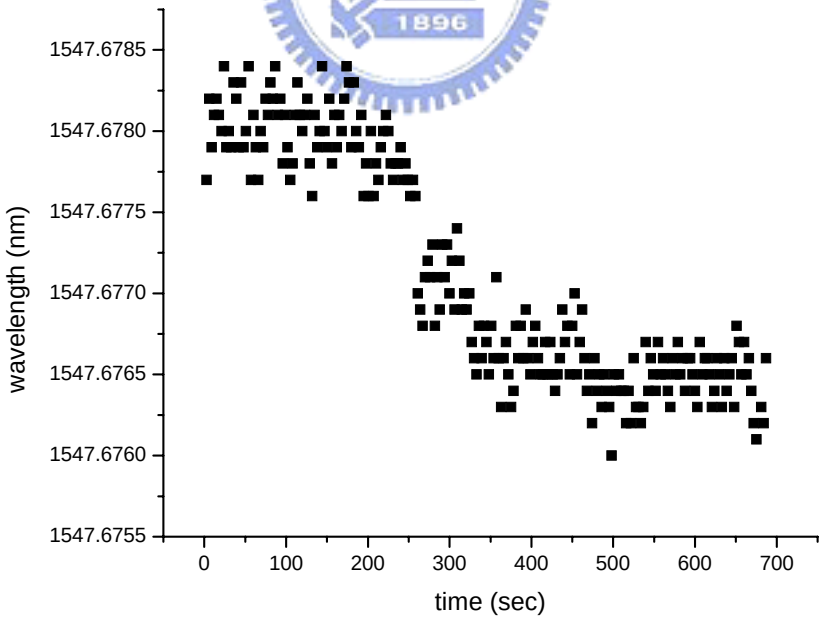

Fig. 3-17 Wavelength shift without stabilization over 10 mins

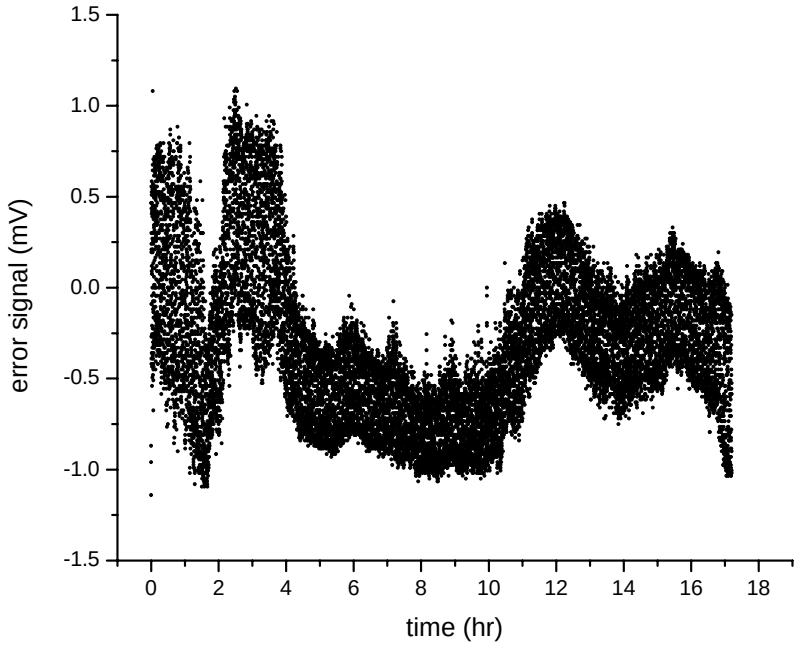

Fig. 3-18 Error signal on stable state over 17 hr

3.3.3 Allan variance

The Allan variance is calculated by

$$\sigma_y^{\,2}(\tau) = \frac{1}{2(N-1)} \sum_{i=1}^{N-1} (f_{i+1} - f_i)^2 / f_0^{\,2}$$

where f_i is a signal frequency averaged over the integration time τ, N is the number of averaged frequencies (f_i), and f_0 is the central optical frequency.

We use this formula to analyze the data of feedback voltage in Fig. 3-14. By choosing different τ value, we can acquire different Allan variance shown in Fig. 3-19. The minimum relative square root of Allan variance is 2.81×10^{-9} for τ value between 1 s and 10 s and by increasing sampling time, the relative square root of Allan variance increases. That means the DFB frequency stability in short-term measurement is better than in long-term measurement.

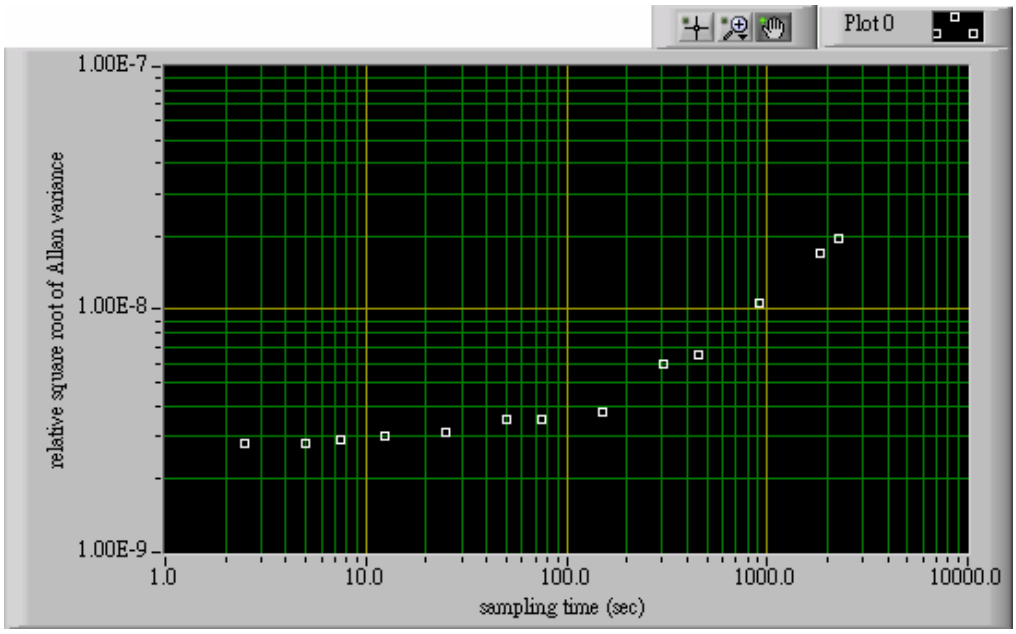

Fig. 3-19 Relative square root of Allan variance by analyzing the data of feedback voltage

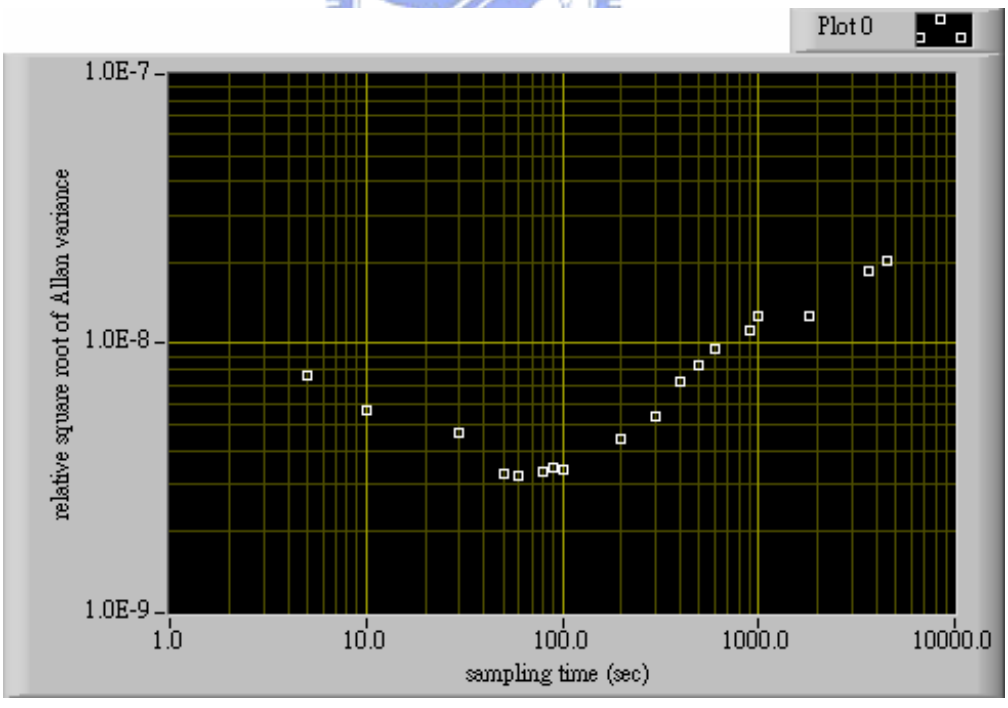

Fig. 3-20 Relative square root of Allan variance by analyzing the data of error signal

We also analyze the data of error signal in Fig. 3-18. Different relative square root of Allan variance corresponding to different τ value is shown in Fig. 3-20. The minimum relative square root of Allan variance in this case is 3.25×10^{-9} for τ = 60 seconds. It increases for both lower and higher sampling time. That means the DFB frequency fluctuation is in the most stable state for a period of 1 minute.

If we just analyze the more stable range (the 4th to the 10th hour) in Fig. 3-18, we can find the minimum relative square root of Allan variance is lower shown in Fig. 3-21. It is 1.9×10^{-9} for τ = 60 seconds.

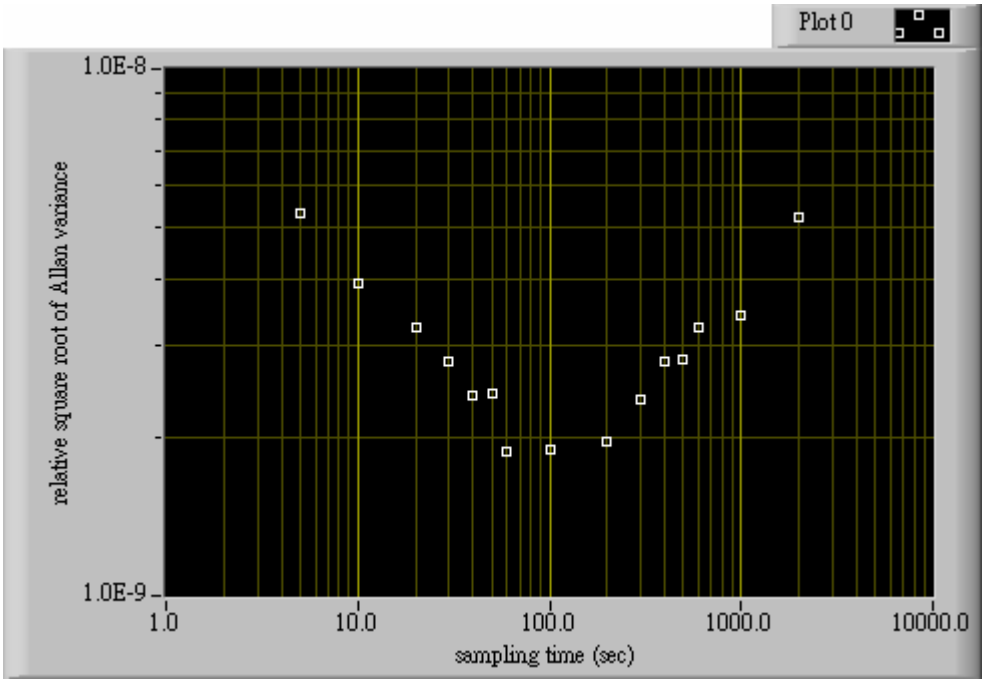

Fig. 3-21 Relative square root of Allan variance by analyzing the data of error signal of more stable period

Chapter 4

Injection locking of external-cavity laser (ECL) by the stabilized DFB laser

In this chapter, we use the stabilized DFB laser that is introduced in chapter 3 to inject to the external-cavity semiconductor laser (ECL) and observe the frequency fluctuation of ECL output wavelength. Sect. 4.1 gives the basic characteristics of ECL; Sect. 4.2 gives the experimental setup. Sect. 4.3 gives the experimental results of injection locking of ECL

4.1 The characteristics of ECL

Owing to its application in optical communication, high-resolution spectroscopy and optical metrology, tunable semiconductor has been extensively studied in past decade. Wavelength selective feedback provided by an external cavity can be used to control the wavelength and narrow the linewidth of a diode laser. Diffraction gratings in external cavity lasers combine the functions of the filter and external mirror. In extended cavity, the light from the grating must be retroreflected back into the gain medium. Two common retroreflecting mounting geometries for diffraction gratings in extended-cavity lasers are the autocollimating (Littrow) configuration and the grazing-incidence (Littman) configuration shown in Fig. 4-1.

In our experiment, we adopt the Littman configuration for our external-cavity semiconductor laser.

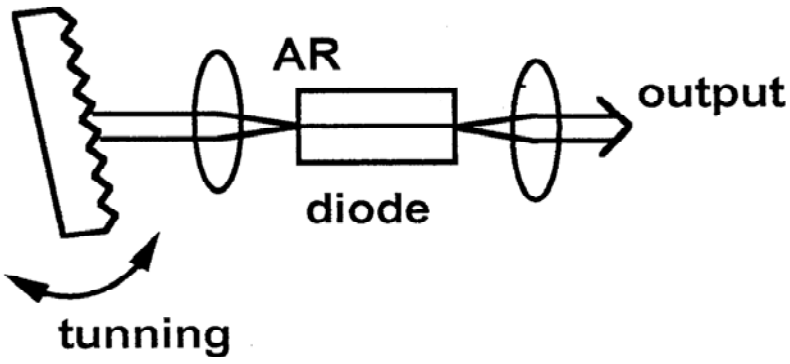

(a)

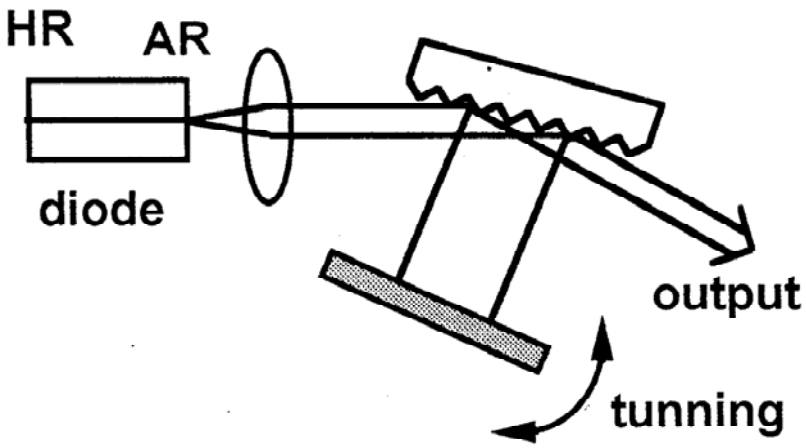

(b)

Fig. 4-1 Two common configurations of ECL: Littrow (a) and Littman (b)

The broadband laser diode we use is Optospeed inc. RSOA067. The L-I curve and the spectrum are shown in Fig. 4-2 and Fig. 4-3, respectively. The threshold current is at 57mA.

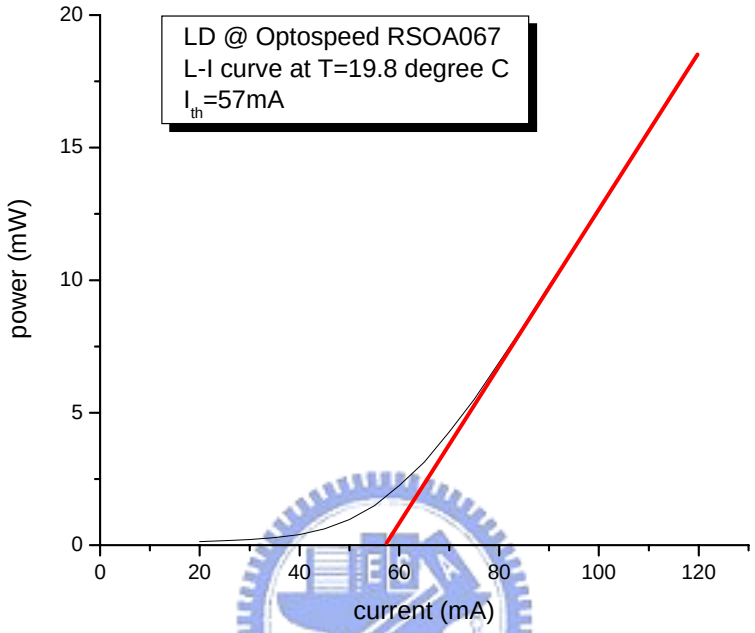

Fig. 4-2 L-I curve of the laser diode without external cavity

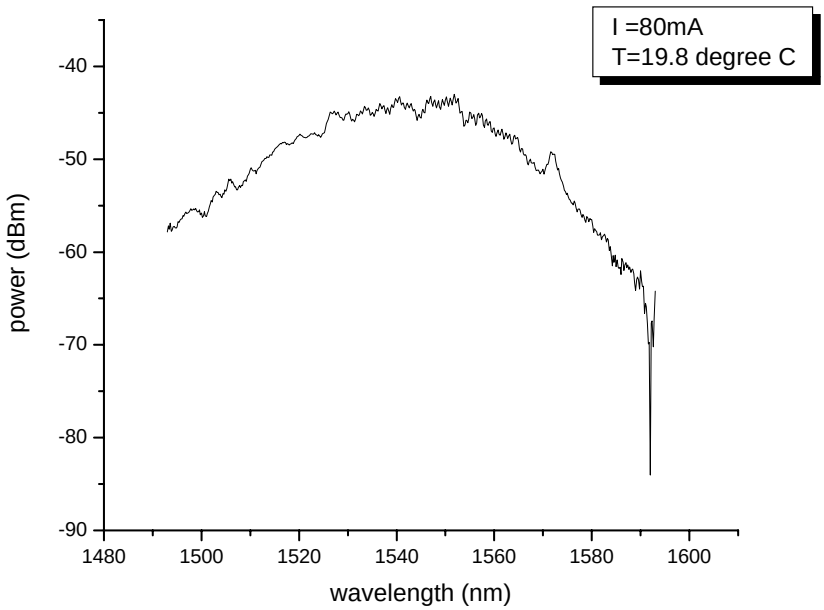

Fig. 4-3 Spectrum of the laser diode without external cavity

Fig. 4-4 and 4-5 show the L-I curve and the spectrum of the laser diode with external cavity. The threshold current of ECL is lower to 52mA.

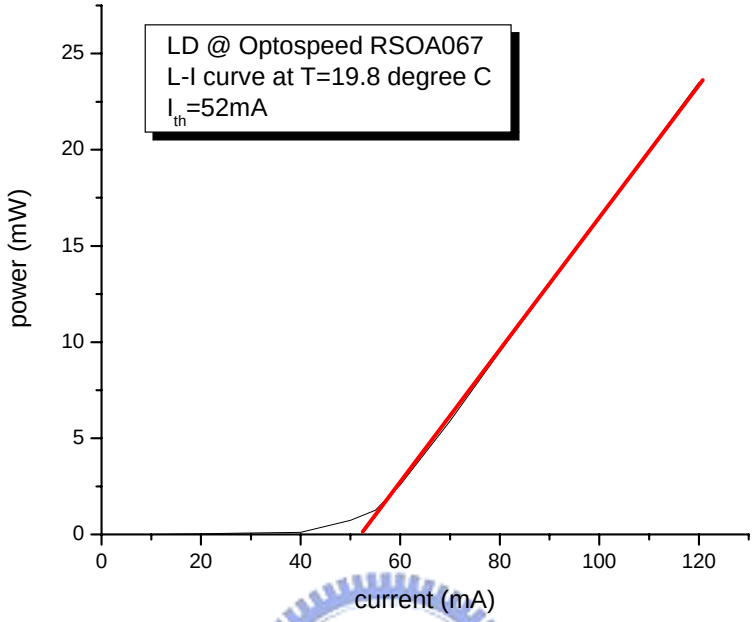

Fig. 4-4 L-I curve of the laser diode with external cavity

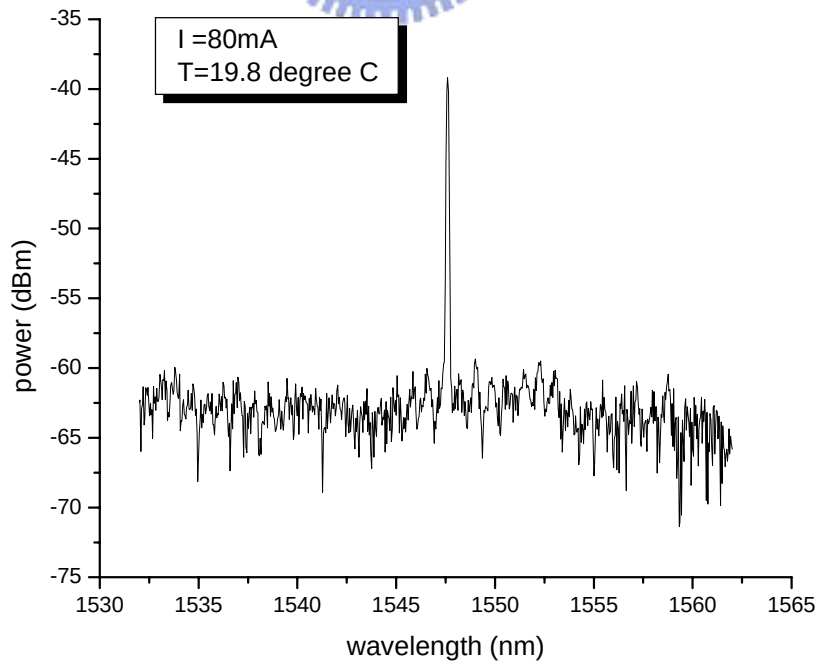

Fig. 4-5 Spectrum of the laser diode with external cavity

4.2 Experimental setup

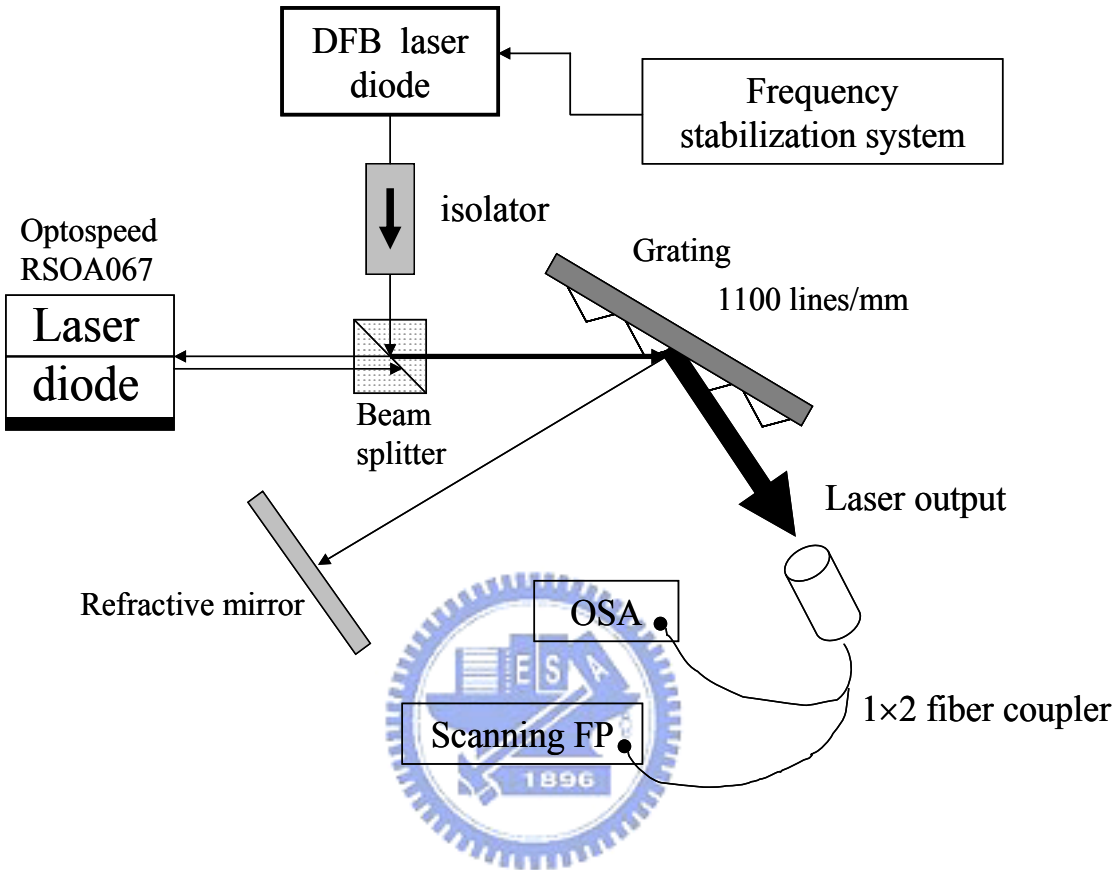

Fig. 4-6 Experimental setup of injection locking of ECL by the DFB laser diode

A schematic diagram of the injection locking of the ECL by the stabilized DFB laser is shown in Fig. 4-6. The output light from master laser (DFB) is sent through a Faraday isolator to prevent any unwanted feedback to the DFB that will affect its stabilized performance. The beam splitter sends part of the output of the DFB to inject into the slave laser (ECL) in Littman configuration. The output of ECL is fiber-coupled to the optical spectrum analyzer with 0.01nm resolution while part of output is coupled to the scanning Fabry-Perot interferometer monitored by an oscillator.

4.3 Experimental results

After injecting the output light of DFB laser diode into the ECL, we can find some special conditions as follows:

4.3.1. ECL is operated below threshold:

We set the driving current of ECL at I = 50mA which is below threshold current (I_{th} =52mA), and then inject the DFB output light into ECL. We find there is a peak appearing in the ECL spectrum shown in Fig. 4-7.

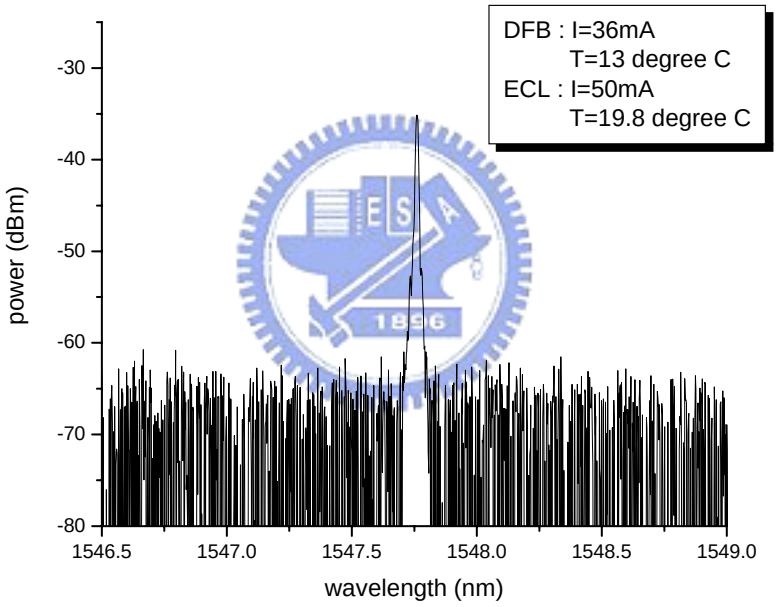

Fig. 4-7 Spectrum of ECL below threshold with DFB injected

When we change the driving current of DFB laser, the wavelength of ECL also changes. Fig. 4-8 shows the results. By increasing the DFB current, the center wavelength of ECL spectrum also increases. The tuning efficiency is 0.0219nm/mA shown in Fig. 4-9. We can compare it to Fig. 3-6 that is DFB self-tuning efficiency. There is just a little difference.

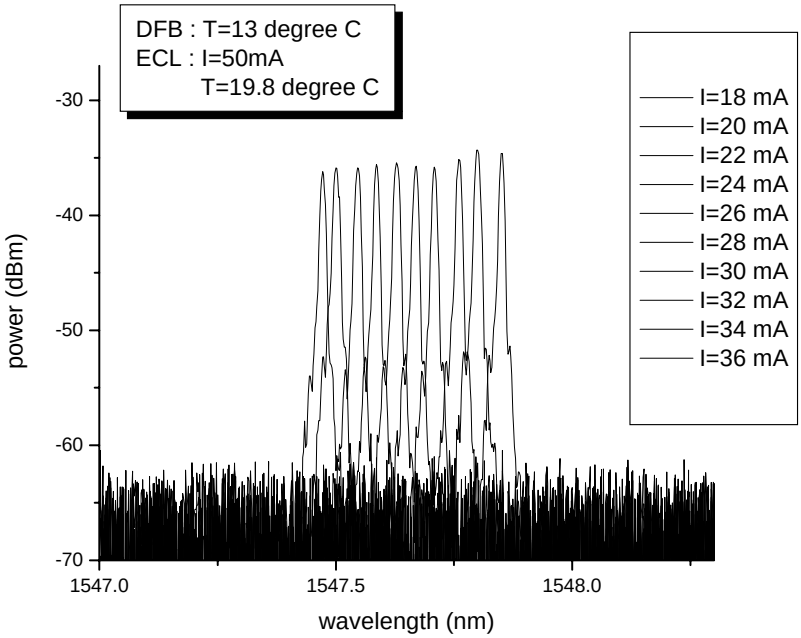

Fig. 4-8 Spectrum of below-threshold ECL with tuning DFB driving current

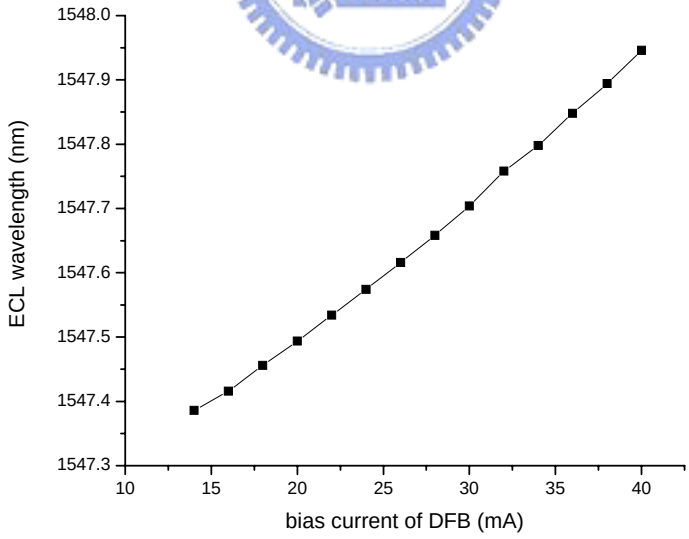

Fig. 4-9 ECL wavelength tuning efficiency by varying the driving current of DFB laser

We use scanning Fabry-Perot interferometer to observe the frequency fluctuation of the ECL output before turning on the DFB frequency stabilization

system. In Fig. 4-10, the peak-to peak frequency fluctuation over 10 minutes is 700MHz.

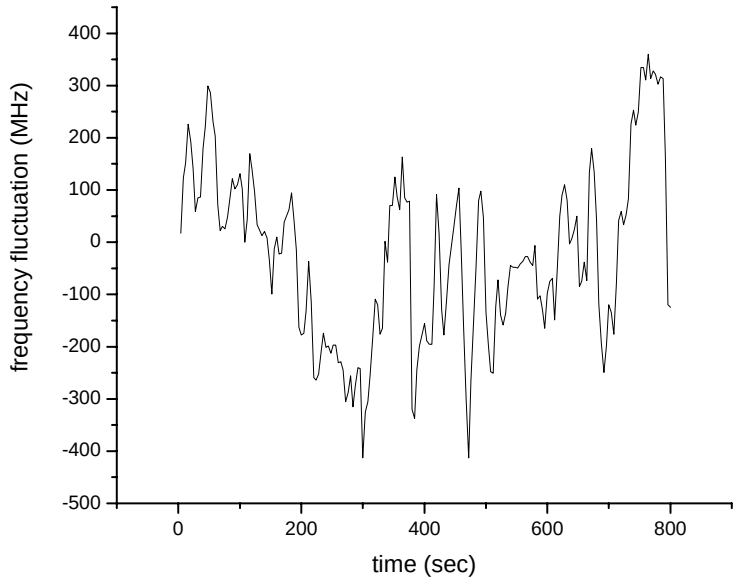

Fig. 4-10 Frequency fluctuation of ECL with unstabilized DFB injection locking

Then we switch the DFB to the stable state and record the ECL frequency fluctuation. We find the peak-to-peak frequency variation is over 300MHz for 1-hour measurement shown in Fig. 4-11.

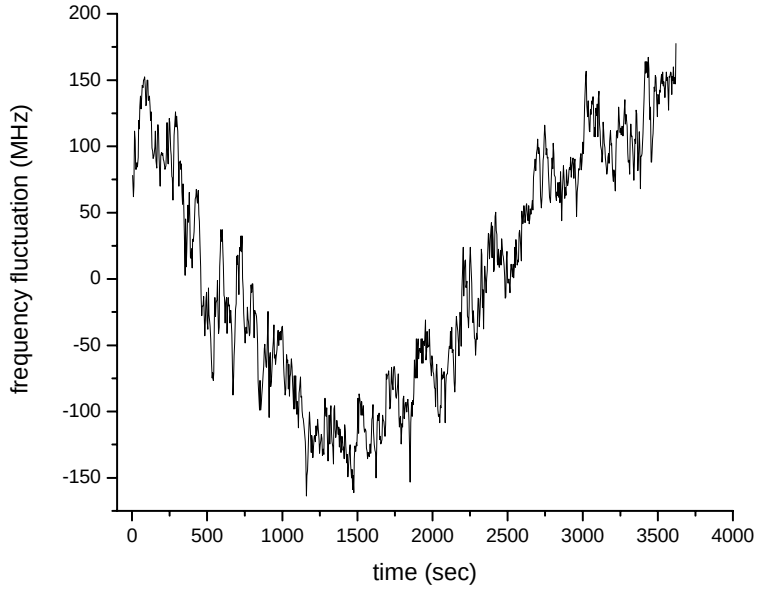

Fig. 4-11 Frequency fluctuation of ECL with unstabilized DFB injection locking

It is quite a large fluctuation. We use the error signal to check the frequency fluctuation of stabilized DFB while the scanning Fabry-Perot interferometer records. The peak-to-peak frequency fluctuation measured by scanning Fabry-Perot interferometer is shown in Fig. 4-12. It is also over 300MHz for a period of 1 hour, but the frequency fluctuation measured by error signal of DFB shown in Fig. 4-13 is only about 23MHz. The calculation for error signal transferring to frequency fluctuation have mentioned in chapter 3.3.1. So we conjecture that the scanning Fabry-Perot interferometer has some drift for a long time measurement.

We use a commercial tunable laser to recheck our scanning Fabry-Perot interferometer. At this time, we also fiber-coupled it to wavemeter to measure its wavelength shift. During same period of time, the frequency fluctuations are quite different shown in Fig. 4-14 and Fig. 4-15. In Fig. 4-14 illustrates the wavelength shifts 0.0012nm ~ Δf = 200MHz in 30 mins. Fig. 4-15 shows the frequency fluctuation is over 1GHz in the same period. These data can prove our scanning Fabry-Perot interferometer has a severe drift.

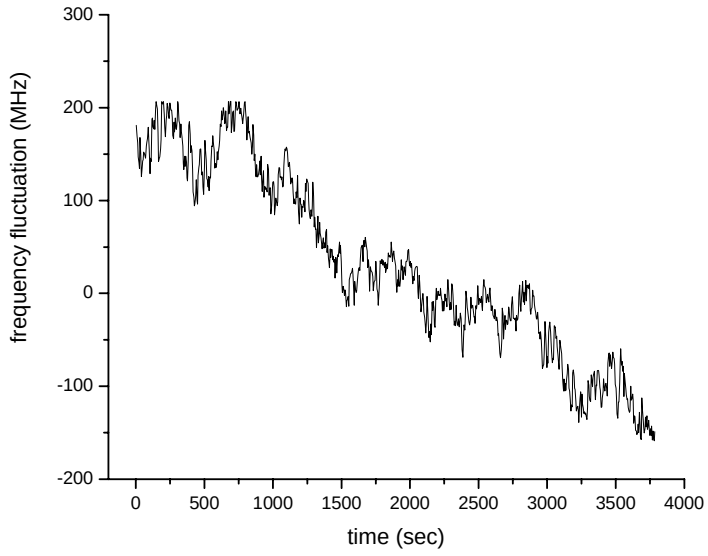

Fig. 4-12 Frequency fluctuation of stabilized DFB laser diode over 1 hour

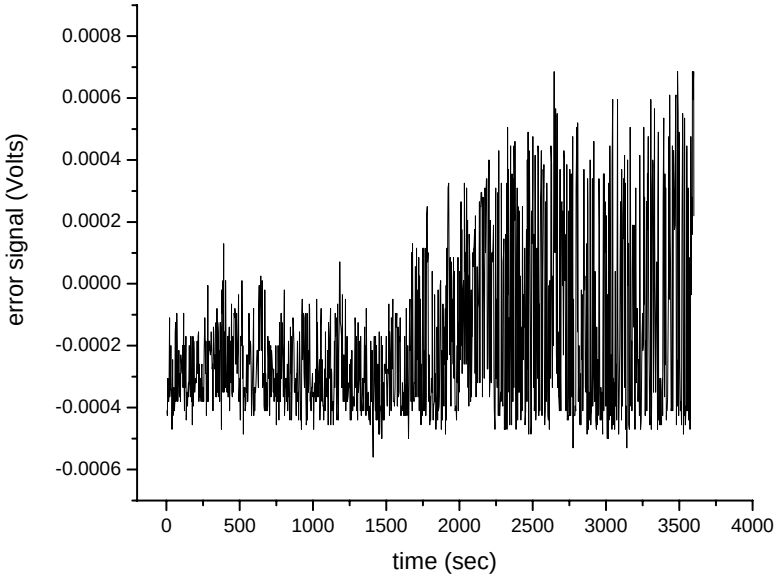

Fig. 4-13 Error signal of stabilized DFB laser diode over 1 hour

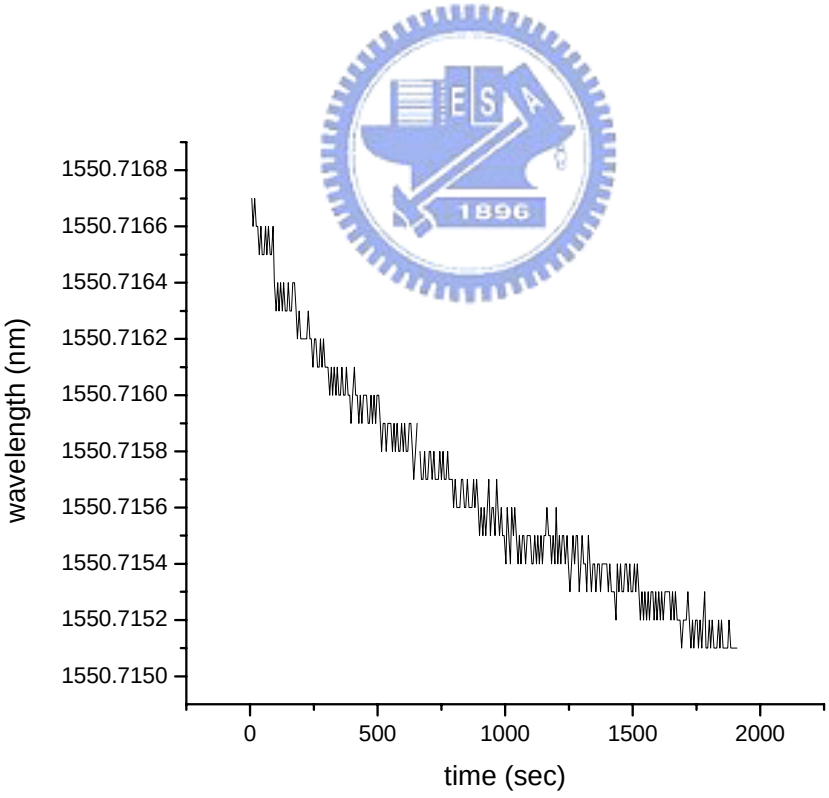

Fig. 4-14 Wavelength variation of the commercial tunable laser measured by wavemeter over 30 mins

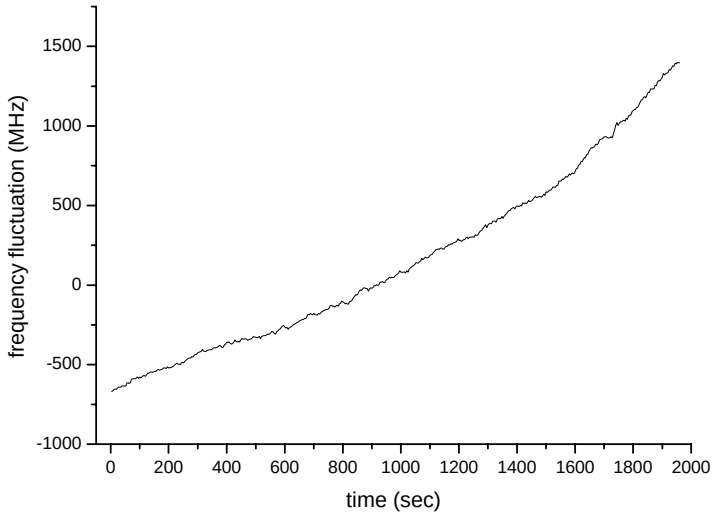

Fig. 4-15 Frequency fluctuation of the commercial tunable laser measured by scanning Fabry-Perot interferometer over 30 mins

Regarding the severe drift of scanning Fabry-Perot interferometer, we figure out some possible reasons. First, the trigger of the oscillator is not very well that will affect the precision of frequency fluctuation. However, after our calculation, the trigger effect leads just 50MHz frequency fluctuation. Second, we conjecture the variation of room temperature causes the FSR of scanning Fabry-Perot interferometer drift. The drift of FSR can be expressed as

$$\boxed{d(FSR) = d(\frac{c}{2L}) = \left|\frac{c\Delta L}{2L^2}\right|} \tag{4-1}$$

$$\boxed{\Delta L = \alpha \Delta T L} \tag{4-2}$$

For our Fabry-Perot interferometer, 1°C temperature variation can lead the cavity length change 70nm. If we assume the room temperature varies 2°C, after calculation, the drift of FSR will be 4KHz. However, this drift is still too small.

Third, we let the Fabry-Perot interferometer be on "non-scanning" state, and observe the DFB output power variation. The result is shown in Fig. 4-16. We can find that the stabilized DFB is always within the linewidth of the non-scanning Fabry-Perot interferometer in a period of 1.5 hr. It is quite reasonable and it infers that the unsure drift is caused by Fabry-Perot interferometer operated at the scanning mode.

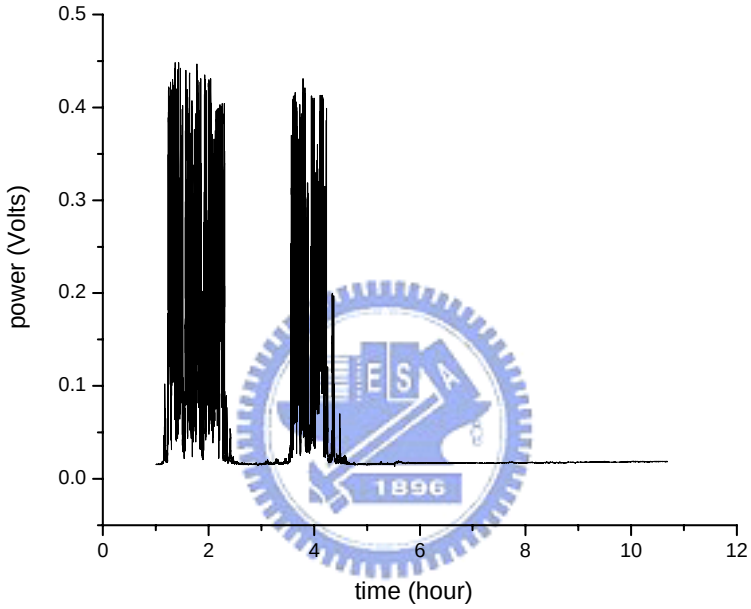

Fig. 4-16 DFB power variation measure by Fabry-Perot interferometer on non-scanning state

We redo the experiment for stabilized DFB laser injecting to the below-threshold ECL. Fig. 4-17 shows the frequency fluctuation measured by scanning Fabry-Perot interferometer and Fig. 4-18 shows the error signal of stabilized DFB laser. Frequency fluctuation is over 300MHz but error signal transferring to frequency is about 30MHz. Compare to Fig. 4-10, one thing we can confirm is the stabilized DFB laser injecting to ECL will let the frequency of ECL output become more stable.

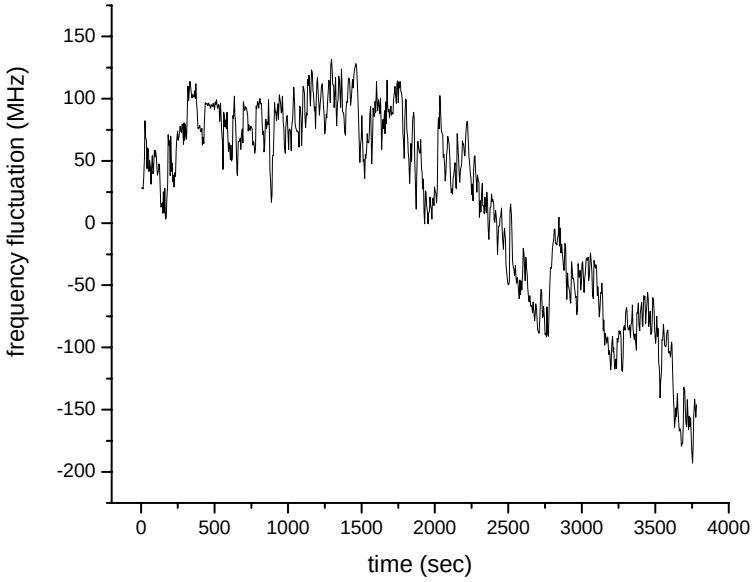

Fig. 4-17 Frequency fluctuation of below-threshold ECL with stabilized DFB injection locking

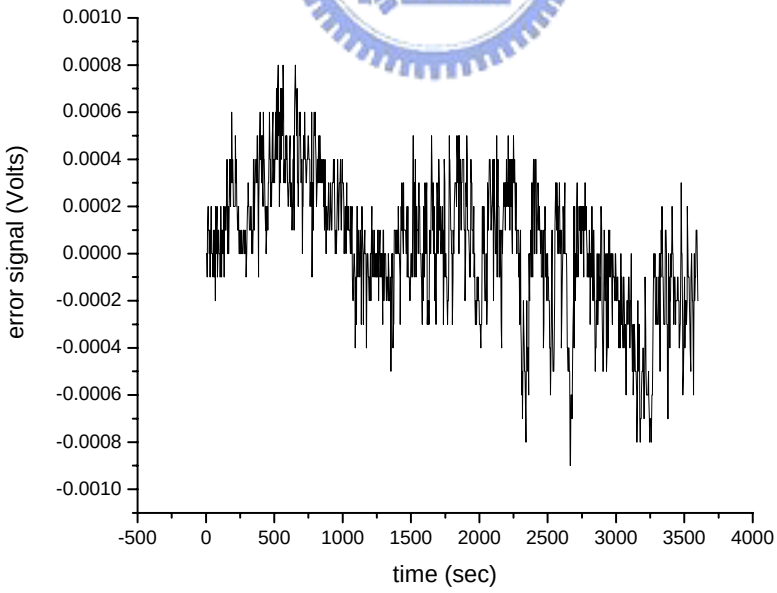

Fig. 4-18 Error signal of DFB while injection locking before-threshold ECL over 1 hour

4.3.2 ECL is operated above threshold:

We set the driving current of ECL at 58.5mA which is above threshold (I_{th} =52mA), then inject DFB laser. Fig. 4-19 shows the spectrum. We find there are two peaks in the spectrum of ECL.

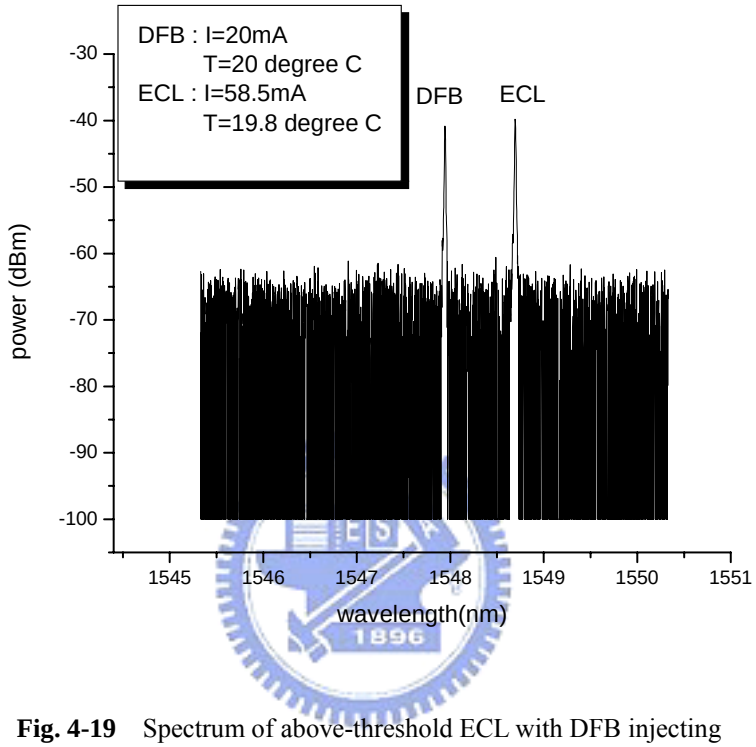

Fig. 4-19 Spectrum of above-threshold ECL with DFB injecting

Then we vary the output wavelength of ECL by tuning the mirror to oscillate close to the wavelength of the DFB laser. When the injecting locking works, the output power of ECL is amplified. We use both optical spectrum analyzer and scanning Fabry-Perot interferometer to observe the phenomenon. Fig. 4-20 shows the only ECL spectrum as blocking DFB laser and Fig. 4-21 shows the only DFB spectrum as blocking ECL. Because the optical spectrum analyzer has lower resolution, we can hardly distinguish between DFB and ECL. Fig. 4-22 shows the injection-locked output amplification of ECL.

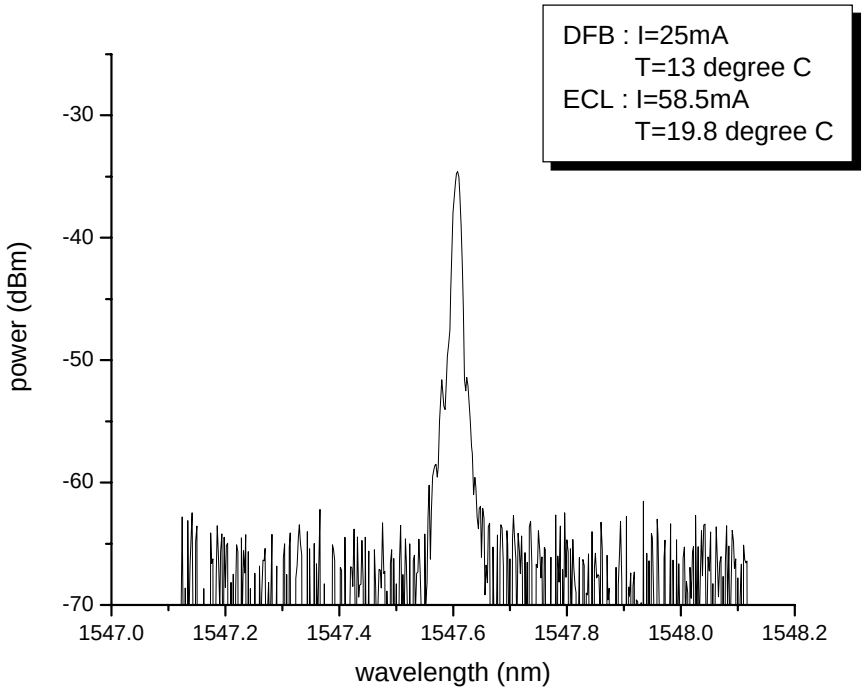

Fig. 4-20 Spectrum of only ECL as blocking DFB laser diode

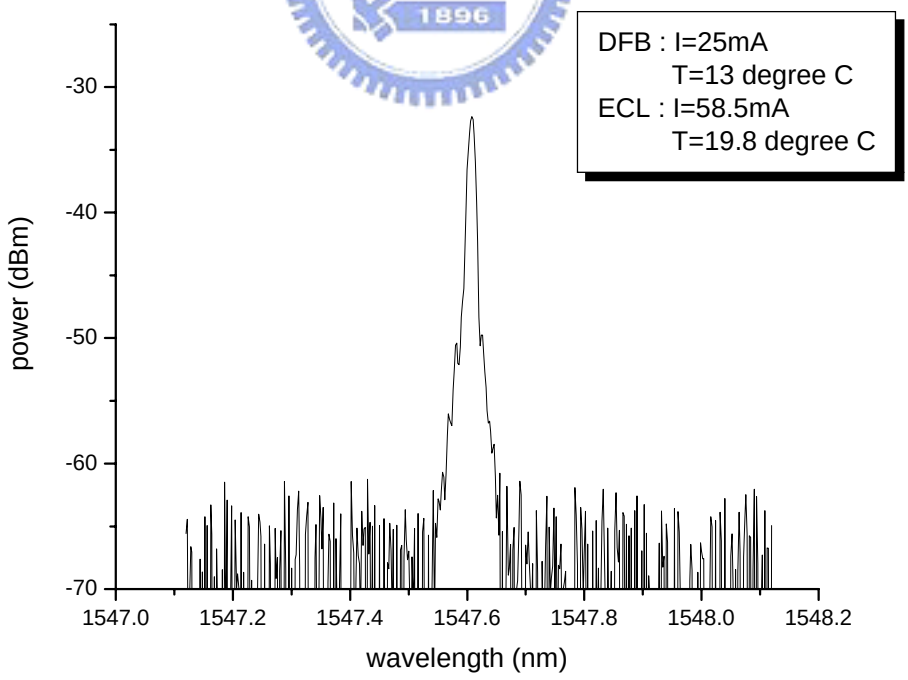

Fig. 4-21 Spectrum of only DFB laser diode as blocking ECL

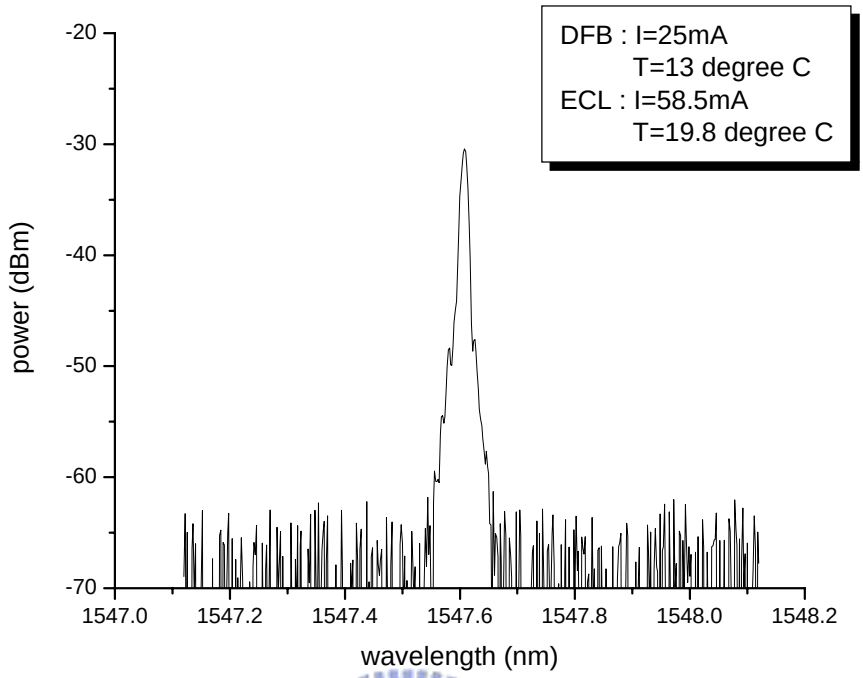

Fig. 4-22 Spectrum of injection-locked ECL by DFB laser

Because scanning Fabry- Perot interferometer has higher resolution, we use it to observe the injecting locking phenomenon. Although the two peak wavelengths are at the same wavelength in optical spectrum analyzer, in scanning Fabry- Perot, they are at quite different positions shown in Fig. 4-23 and Fig. 4-24. Fig. 4-25 shows the results of injection locked ECL by using DFB laser. The same as Fig. 4-22, the intensity is amplified. Compared Fig. 4-25 to Fig. 4-23 and 4-24, the injection-locked output wavelength of ECL is quite at the DFB wavelength.

In order to assure that the ECL output wavelength is really locked by DFB laser, we changes the DFB driving current. The result is shown in Fig. 4-26. The FSR of ECL is 2GHz and then we can calculate the ECL shifts about 350MHz when the driving current of DFB changes 0.1mA.

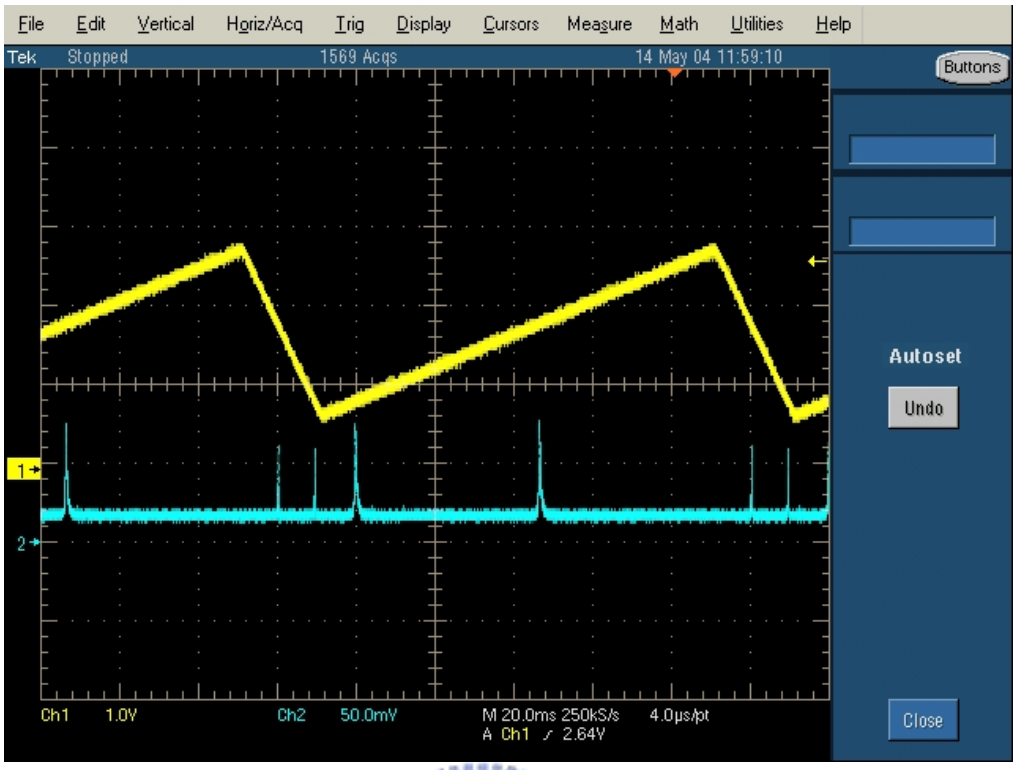

Fig. 4-23 Result of scanning Fabry-perot interferometer of only ECL as blocking DFB laser diode

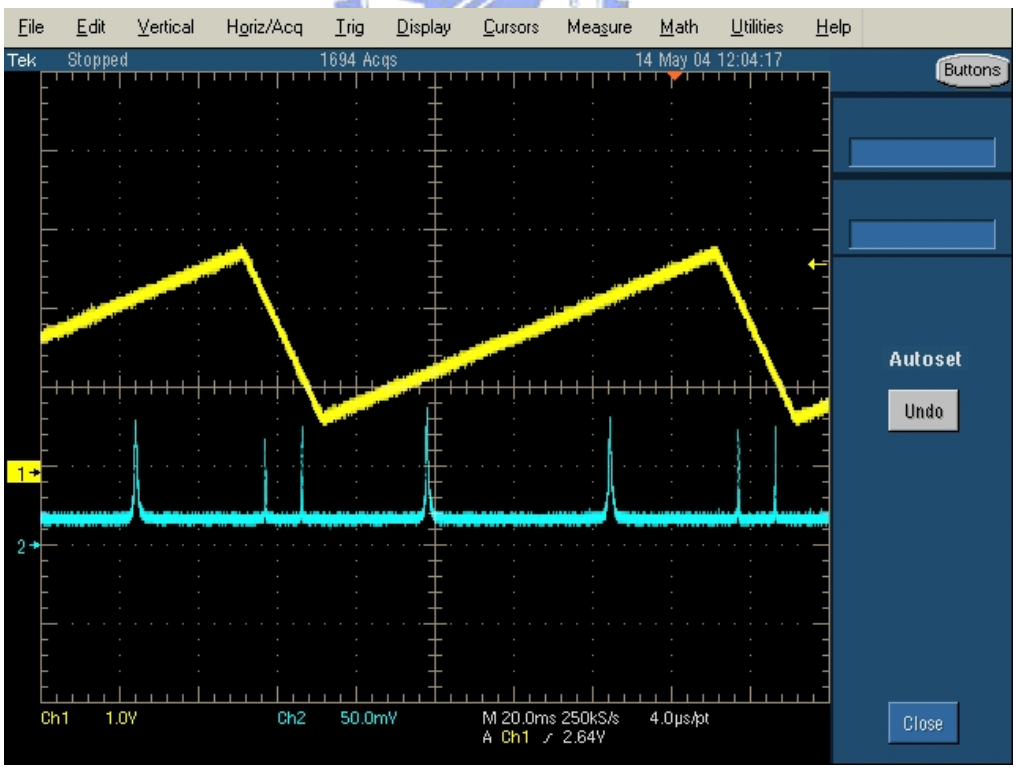

Fig. 4-24 Result of scanning Fabry-perot of interferometer only DFB laser diode as blocking ECL

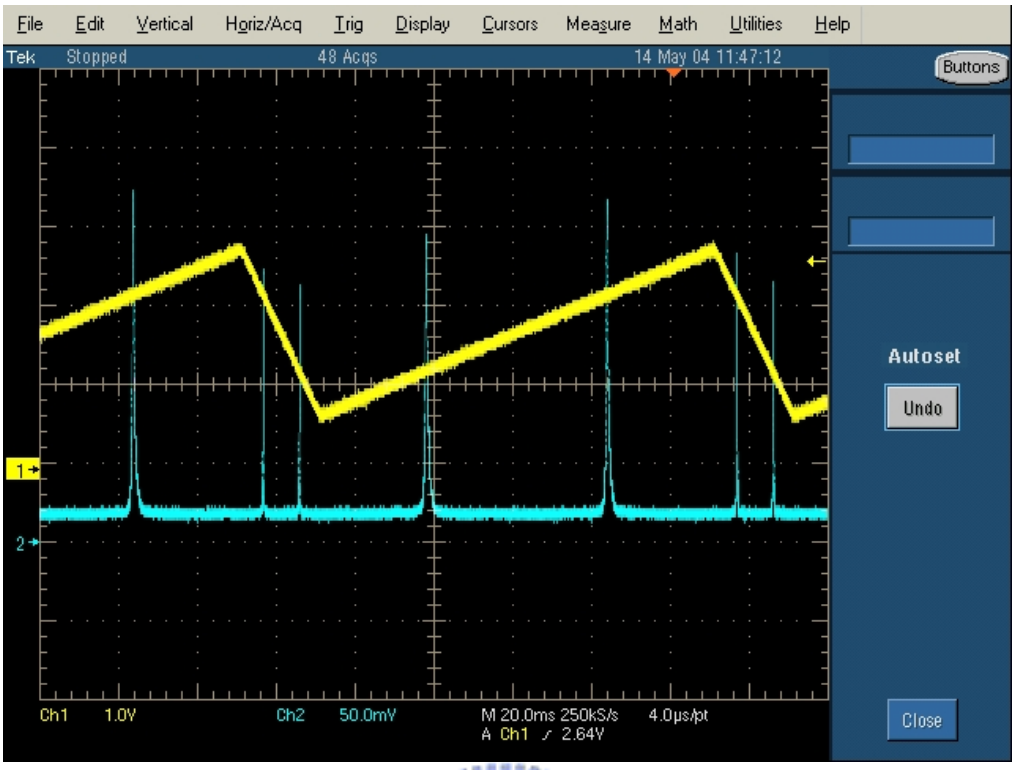

Fig. 4-25 Scanning Fabry-perot interferometer results of injection-locked ECL by using DFB laser diode

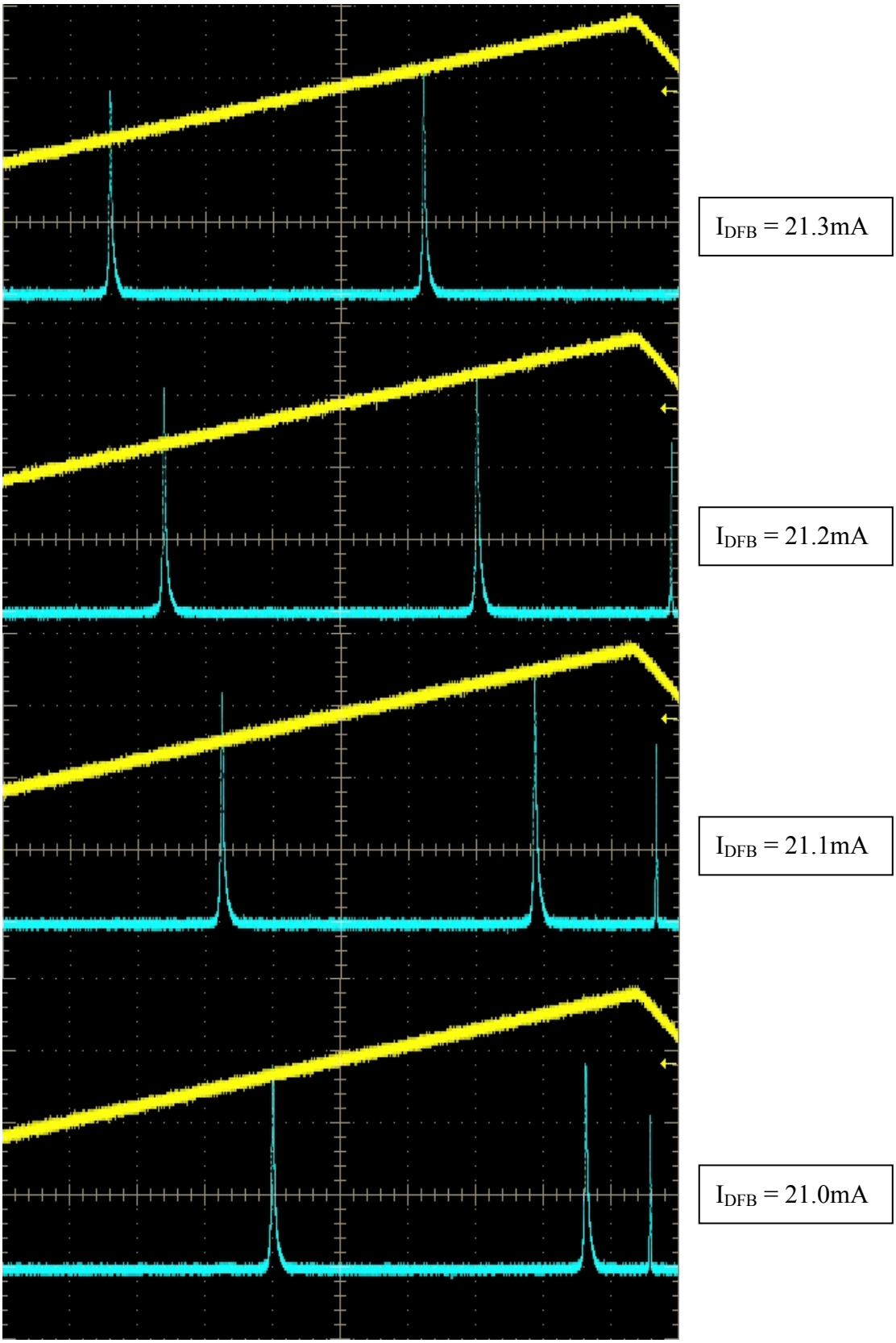

Fig. 4-26 Observation of ECL output wavelength as tuning DFB drrving current

Then we switch the DFB to stable state and record the ECL frequency fluctuation. It is shown in Fig. 4-27. We find in the beginning (about 20 minutes) of the injection locked of ECL, the frequency fluctuation is about 200MHz. But 20 minutes later, the waveform begins to split into two modes.

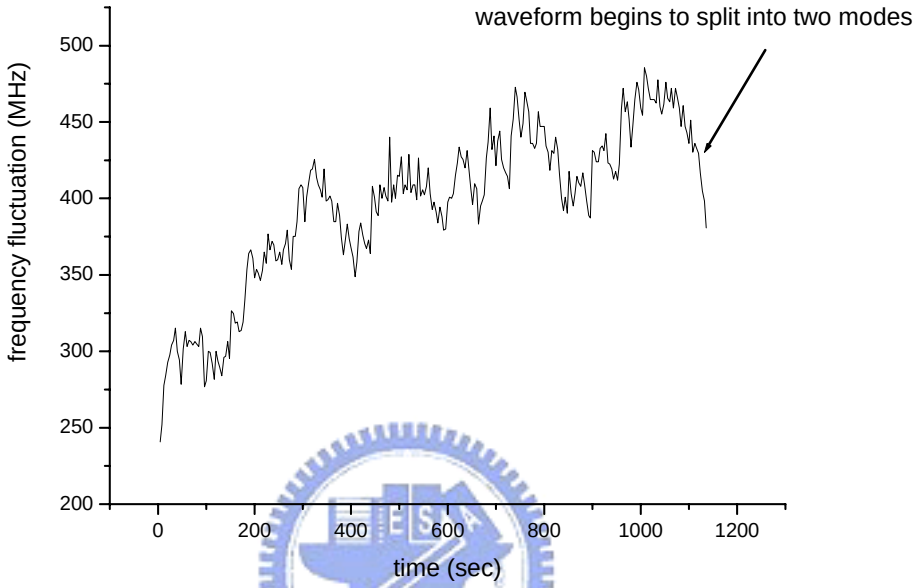

Fig. 4-27 Frequency fluctuation of above-threshold ECL with stabilized DFB injection locking

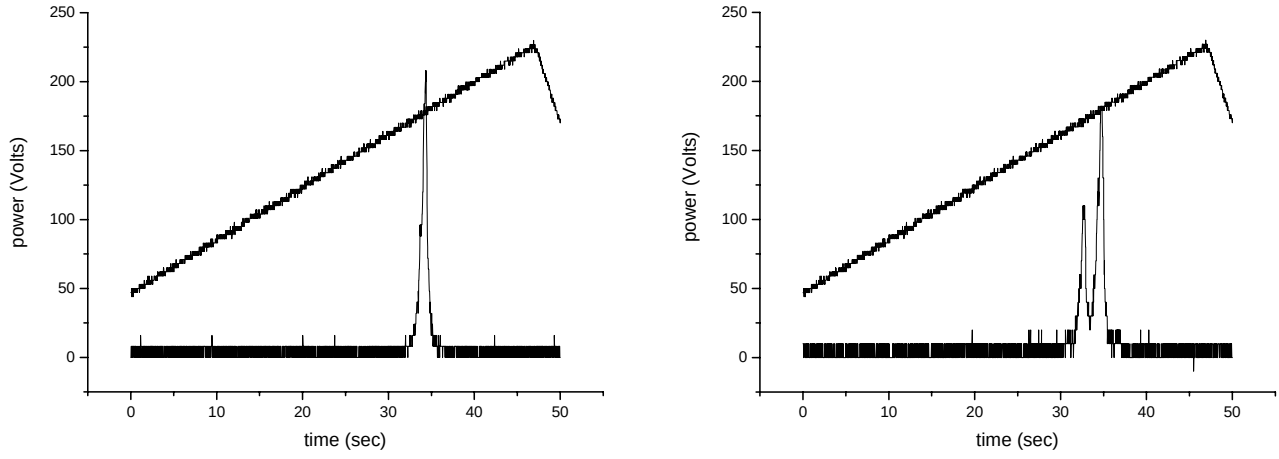

(a) (b)

Fig. 4-28 (a) in the beginning of injecting locking of above-threshold ECL (b) 20 minutes later after injecting locking of above-threshold ECL

Fig. 4-28 (a) shows the graph of scanning Fabry- Perot interferometer in the beginning of injection locking of above-threshold ECL and after 20-minute measurement; we find the waveform split into two modes shown in Fig. 4-28 (b).

We speculate that the ECL competes with the DFB. Moreover, we guess ECL is mode hopping that leads the waveform division. So we measure the frequency fluctuation of ECL for at least one hour shown in Fig. 4-29. ECL is mode hopping after half an hour. We also measure the room temperature at the same time shown in Fig. 4-30.

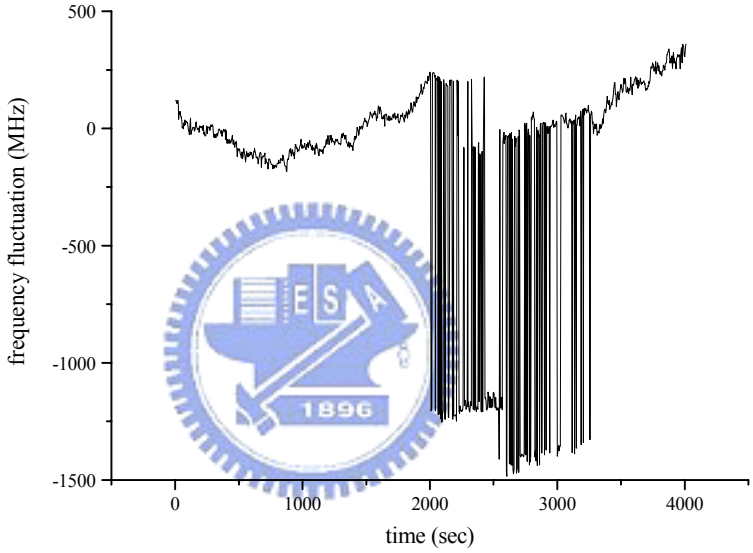

Fig. 4-29 Frequency fluctuation of ECL over 1 hour measurement

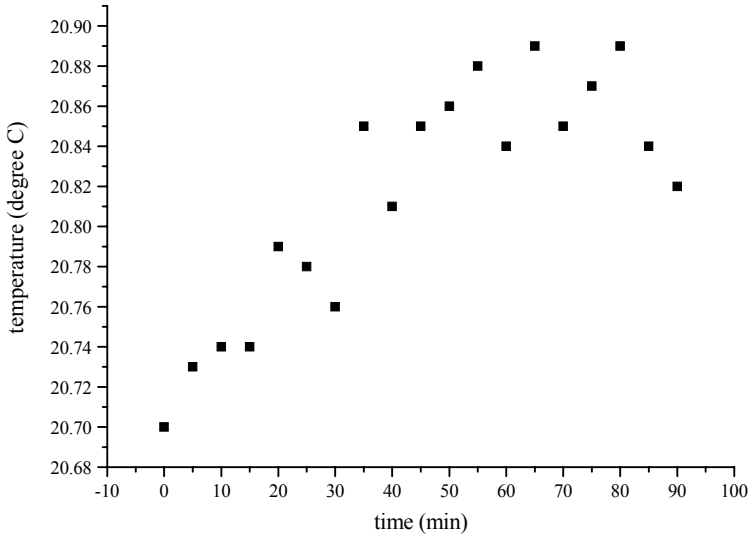

Fig. 4-30 Temperature variation while recording the frequency fluctuation of ECL

Fig. 4-31 also shows the frequency fluctuation of injection locking of above-threshold ECL but at this time, we tune the mirror of ECL when we see the waveform splitting into modes. The waveform splits three times for 1-hour record. The error signal of DFB is also measured by multimeter at the same time shown in Fig. 4-32.

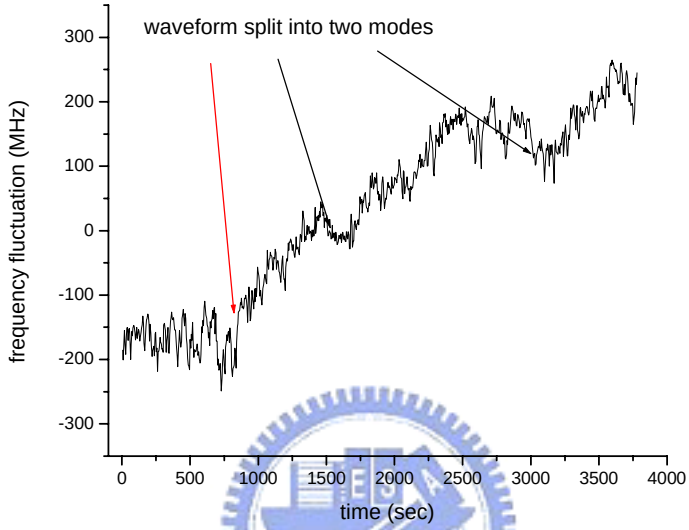

Fig. 4-31 Frequency fluctuation of above-threshold ECL with stabilized DFB injection locking over 1 hour

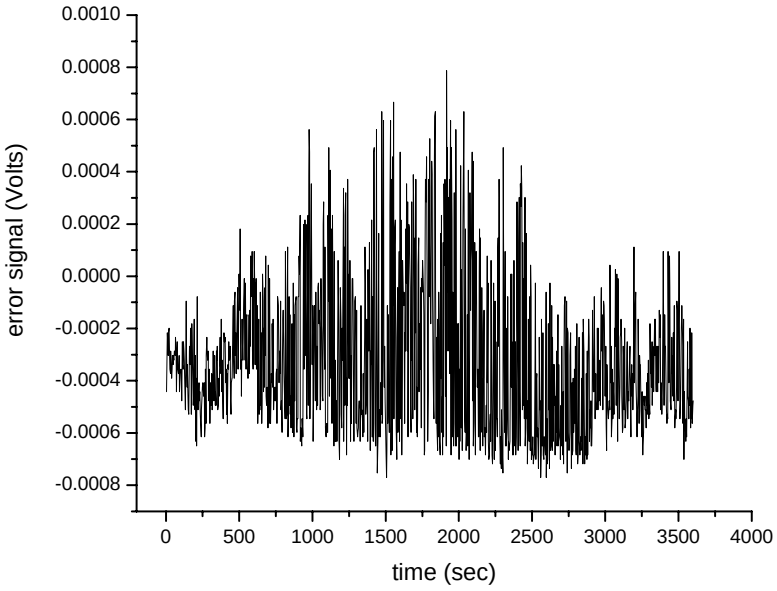

Fig. 4-32 Error signal of DFB while injection locking above-threshold ECL over 1 hour

Chapter 5

Conclusions

5.1 Conclusions

Because of its low cost and simple setup, DFB laser diode is widely used as a light source for WDM optical communication systems. Its wavelength, however, varies with temperature and injection current. This would result in degrading transmissions of adjacent channels by optical crosstalk. Therefore, frequency stabilization is important for this laser. In this thesis, we demonstrate a simple method for frequency stabilization of a DFB laser that uses a fiber Bragg grating. It is based on a level detection technique using the transmission and non-transmission profiles of the FBG. The frequency of the DFB laser is locked to the side of the transmission profile of the fiber grating. The error signal is feedback to control the driving current of the laser. In our experimental results, the frequency fluctuation of the DFB laser LD reduced to less than 30 MHz after stabilization for a period of one hour. It is improved by an order of magnitude compared with the free-run state. For long-term measurement over 17 hours, the frequency fluctuation is less than 50MHz. The square root of the Allan variance is 3.25×10^{-9} at sampling time of 60s.

At the second part of our experiment, we injection locked the ECL by using our stabilized DFB laser diode. When the ECL is operated at $I/I_{th}=0.96$ below threshold, from the error signal, we get the frequency fluctuation of ECL is about 23MHz for one hour record. For driving-above-threshold ECL, the waveform of ECL will split into two modes because the ECL competes with the DFB laser.

5.2 Future work

To avoid the competition between ECL and DFB, we can use semiconductor amplifier or EDFA to amplify the output power of the master laser (DFB laser) to increase injection locking efficiency.

In addition, we will try to replace the reflected mirror of ECL with a stripe mirror to produce dual wavelength output or with a liquid crystal pixel mirror (LCPM) to produce multiple wavelength output. We expect that when we lock one of the output wavelengths, the others will also be locked. Moreover, we can lock the stabilized DFB laser to a group of optical comb, and injection locking to a DWDM system.

Reference

[1] M. Chbat and D. Penninck, "High-spectral-efficiency transmission systems," in *optical Fiber Conf. (OFC2000)*, 2000, pp. 134-136.

[2] Bruce Nyman, Mark Farries, and Calvin Si. "Technology Trends in Dense WDM Demultiplexers." *Optical Fiber Technology*, vol 7, pp. 255-274, 2001

[3] Leonid Kazovsky, Sergio Benedetto, Alan Willner, " Optical fiber communication systems (University Science Book, *Artech House Pulishers.*, 1999)

[4] Y.C. Chung, K.J. Pollock, P.J. Fitzgerald, B. Glance, R.W. Tkach, and A.R. Chraplyvy, *Electronics Lett*., vol. 24, pp. 1313, 1988

[5] S. Sudo, Y. Sakai, H. Yasaka, and T. Ikegami, "Frequency-stabilized DFB module using 1.53159 _m absorption line of C2H2," *IEEE Photon. Technol. Lett.,* vol. 1, pp. 281–284, Oct. 1989.

[6] Youngil Park, Seung-Tak Lee, and Chang-Joon Chae, "A novel wavelength stabilization scheme using a fiber grating for WDM transmission," *IEEE Photon. Technol. Lett.,* vol. 10, pp. 1446–1448, Oct. 1998.

[7] S. T. Winnall,, and A. C. Lindsay ,"DFB semiconductor diode laser frequency stabilization employing electronic feedback and Bragg Grating Fabry–Perot interferometer," *IEEE Photon. Technol. Lett.,* vol. 11, pp. 1357–1359, Nov. 1999.

[8] F. Favre, D. LeGuen, and J. C. Simon, "Optical feedback effects upon laser diode oscillation field spectrum," *IEEE J. Quantum Electron.,* vol. QE-18, pp. 1712–1717, 1982.

[9] Turan Erdogan, "Fiber Grating spectra," *IEEE J. Lightwave Technol*., vol. 15, pp. 1277-1294, 1997.

[10] Lam, D.K.W., and B.K. Garside, "Characterization of signal-mode optical fiber filters,"*Applied Optics*, vol.20,pp. 440-445, 1981.

[11] Andreas Othonos, Kyriacos Kalli, "Fiber Bragg Gratings--Finsamentals and Applications in Telecommunications Telecommunications and Sensing A" (University Science Book, *Artech House Pulishers.*, 1999).

[12] A. E. Siegman, Lasers (*University Science Book*, Mill Valley, Calif.,1986).

[13] M. R. Sureete, D. R. Hjelme, R. Ellingsen, and A.R. Mickelson, "Effects of noise on transients of inkection locked semiconductor lasers", *IEEE J. Q. E.,* Vol. 29, No. 4, pp. 1046-1063, 1993

[14] B. Van der Pol, "Forced oscillations in a circuit with nonlinear resistance ", *Phil. Mag*., Vol. 3, pp. 65-80, 1927.

[15] R. Adler, “A study of locking phenomena in oscillators”, *Proc. IRE.*, Vol. 34, pp.351-357, 1946

[16] H. Stover and W. Steiner, “Locking of Laser oscillators by light injection”, *Appl. Phys. Lett.*, Vol. 8, pp. 91-93, 1966.

[17] C. Buczek. R. Freilberg, and M. Sknolnick, “Laser injection locking” *Proc. IEEE*. Vol. 61 pp. 1411-1431, Oct. 1973

[18] Kobayashi and T. Kimura, “Coherence of injection-locked AlGaAs semiconductor laser,” *Electron. Lett.*, Vol. 16, pp. 668-670, Aug. 1980.

[19] S. Kobayashi, J. Yamada, S.Machida, and T. Kimura, “Single-mode operation of 500Mbit/s modulated AlGaAs semiconductor laser by injection locking”, *Electron. Lett.*, vol. 16, pp. 746-748, 1980.

[20] K. Otsuka and S. Tarucha, “Theoretical studies on injection induced modulation of laser diodes”, *IEEE J. Q. E.,* Vol. 17, No. 8, pp. 1515-1521, 1981

[21] R. Lang, “Injection locking properties of a semiconductor laser,” *IEEE J. Q. E.,* vol. QE-18, pp. 976–983, June 1982.

[22] Y. Yamamoto, and T. Kimura, “Coherent optical fiber transmission systems”, *IEEE J. Q. E.,* vol. 17, pp. 919–935, 1981.

[23] C. H. Henry, N. A. Olsson, and N. K. Dutta, “Locking range and stability of injection locked 1.54 _m InGaAsP semiconductor laser,” *IEEE J. Quantum Electron.,* vol. QE-21, pp. 1152–1156, Aug. 1985.

[24] K. Kikuchi and C. Zah, “Spectral, phase noise and phase modulation characteristics of AM sideband injection-locked semiconductor laser,” *Electron Lett.,* vol. 23, No. 4, pp. 437–439, 1987.

[25] I. Petitbon, P. Gallion, G. Debarge, and C. Chabran, “Locking bandwidth and relaxation oscillation of an injection-locked semiconductor laser,” *IEEE J. Quantum Electron.,* vol. 24, No. 2, pp. 148–154, Feb. 1988.

[26] M. R. Surette, D. R. Hielme, R. Ellingsen, and A. R. Mickelson, “Effects of noise on transition of injection locked semiconductor lasers,” *IEEE J. Quantum Electron.,* vol. 29, No.4 pp. 1046–1063, Apr. 1993.

[27] J. Wang, M. K. Halder, L. Li, and F. V. C. Mendis, “Enhancement of modulation bandwidth of laser diodes by injection locking,” *IEEE Photon. Technol. Lett.,* vol. 8, No. 1, pp. 34–36, Jan. 1996.

[28] G. Yabre, “ Effect of relative strong light injection on the chirp-to-power ratio and 3-dB bandwidth of directly modulated semiconductor lasers,” *J. Lightwave Technol.,* Vol. 14, No. 10, pp. 2367–2373, Oct. 1996.

[29] J. M. Liu, H. F. Chen, X. J. Meng, and T. B. Simpson, “Modulation bandwidth, noise and stability of a semiconductor laser subject to strong injection locking,” *IEEE Photon. Technol. Lett.,* Vol. 9, No. 10, pp. 1325–1327, Oct.

1997.

[30] K. H. Seng, M. K. Haldar, and F. V. C. Mendis, “Effect of injection level and detuning frequency on intensity modulation response of an injection-locked semiconductor laser,” in *Proc. 3rd Asia–Pacific Conf. Communications,* Sydney, Australia, 1997, pp. 663–666.

[31] F. Mogensen, H. Olesen, and G. Jacobsen, “Locking conditions and stability properties for a semiconductor laser with external light injection”, *IEEE J. Quantum Electron.,* vol. 21, pp. 784 –793, 1985.